Optimization of ANC Feedback Filters

Master Thesis by

Manuel Brandner

Graz 2014

Host Institution:
Institute of Electronic Music and Acoustics
University of Music and performing Arts Graz

Graz University of Technology

Supervisors: Dipl.-Ing. Markus Flock, PhD
Dipl.-Ing. Dr.techn. Alois Sontacchi
Assessor: O.Univ.Prof. Mag.art. DI Dr.techn. Robert Höldrich

institut für elektronische musik und akustik

Statutory Declaration

I declare that I have authored this thesis independently, that I have not used other than the declared sources/resources and that I have explicitly marked all material which has been quoted either literally or by content from the used sources.

Graz,

....

Eidesstattliche Erklärung

Ich erkläre an Eides statt, dass ich die vorliegende Arbeit selbstständig verfasst, andere als die angegebenen Quellen/Hilfsmittel nicht benutzt und die den benutzten Quellen wörtlich und inhaltlich entnommenen Stellen als solche kenntlich gemacht habe

Graz am,

....

Abstract

Headphones with active noise control reduce unwanted environmental noise via anti-noise, which is the phase inverted noise signal. The anti-noise is subtracted from the noise signal. One efficient method is to record the residual noise at the outer ear canal (therefore inside the ear cup) and feed it back to the headphones speaker. The feedback loop is only stable for phase shifts below 180°. The frequencies where this phase shift occurs are dependent on the construction and use of the headphones (e.g. contact pressure, etc.) and needs to be damped by the ANC-filter. The first task of this diploma thesis is to find a measurement procedure to evaluate the possible worst case scenarios in headphone use. The second task is the optimization of the ANC-filter in respect of the analyzed measurement data. The final task is to optimize the found solution for a limited filter order system.

Kurzfassung

Kopfhörer mit aktiver Geräuschunterdrückung (engl. active noise control: ANC) reduzieren Umgebungslärm indem sie einen phaseninvertierten Antilärm abspielen, der mit dem Lärm destruktiv interferiert. Eine effiziente Methode ist es, den Restlärm direkt am Ohreingang (also im Kopfhörer) aufzunehmen und an den Lautsprecher rückzukoppeln. Die Rückkopplung ist aber nur stabil, solange es zu keiner Phasenverschiebung von weiteren 180° kommt. Die Frequenz, bei der es zu einer Phasenverschiebung von 180° kommt, hängt von der Beschaffenheit und Anwendung des Kopfhörers (Anpressdruck etc.) ab und muss durch das ANC-Filter gedämpft werden. Der erste Schritt dieser Diplomarbeit ist es deshalb, eine Messprozedur zu erarbeiten, die die "worst-case" Szenarien der Kopfhörerbenutzung abbilden. Im zweiten Schritt wird auf der Basis dieser Messungen eine automatisierte Optimierung des ANC-Filters erarbeitet. Im dritten Schritt wird diese Optimierung unter Berücksichtigung einer vorgegebenen Filterordnung angepasst.

Danksagung

Als erstes möchte mich vor allem bei meinem Betreuer Markus Flock für die motivierenden Worte und die vielen anregenden Diskussionen bedanken, die es ermöglicht haben diese Arbeit in diesem Ausmaß und Qualität zu erstellen. Danke, deine Arbeit als Betreuer gab mir ausreichend Energie um diese Masterarbeit mit viel Motivation und Enthusiasmus zu schreiben.

Ich möchte mich auch bei Alois Sontacchi für die sehr gute Vorbereitung auf die Masterarbeit durch die Betreuung meiner Bachelorarbeit und meines Toningenieur-Projektes bedanken, welche den Weg für diese Arbeit geebnet hat.

Weiters möchte ich mich auch bei den Mitarbeitern des Instituts für Elektronische Musik und Akustik bedanken, die immer ein offenes Ohr für fachliche Fragen von mir hatten. Es gab einige.

Ich möchte ich mich bei meiner ganzen Familie, besonders bei meiner Mutter und auch meiner Großmutter, für die große Unterstützung während und auch vor meines Studiums bedanken. Ohne euch wäre mein bisheriger Werdegang niemals möglich gewesen!

Ich bedanke mich auch bei meiner Lebenspartnerin Klaudia. Danke, dass du immer ein offenes Ohr für mich gehabt hast und mich in dieser turbulenten Lebenslage unterstützt und auch immer wieder motiviert hast.

Contents

Chapter 1

Introduction

1.1 ANC - Active Noise Control

The topic of noise control and reduction is a vast field for scientific research. The first patent for a noise control system dates back to the year 1936 [Lue36]. Ever since, the control of noise in different environments has been explored. Ambient noise can be distractive, leading to a loss of concentration or even hearing damage. On the one hand, improvement in better damping of the housing of a radiating noise source and on the other hand hearing protection can be used as a salvation for noise problems. In some cases, only the latter one is possible. That is why common active noise control is used to reduce ambient noise in modern headphones. In nowadays noise-canceling headphones we also find combinations of different noise control approaches. The common approaches for ANC are the feedback noise control and feed forward noise control. The hybrid approach combines these two and all of their advantages.

1.2 Feedback Control

In the case of a feedback control the audio signal of the headphones and the ambient noise predominant inside a headphone ear-cup are fed to a feedback-loop. The ambient noise and the audio signal, which overlap acoustically inside the ear-cup, are picked up via a microphone placed close to the headphone loudspeaker. The audio signal is then subtracted from the picked up signal. The remaining noise is send to the feedback loop where it is shaped by a filter. The approach is also

referred to as closed-loop shaping in control system theory. The feedback-loop has to meet certain stability constraints to work properly which will be discussed later. This approach is common in reduction of narrow band noise for frequencies below 1 kHz and uses the advantage of noise reduction for high frequencies due to passive damping of the headphone ear-cups.

1.3 Feed Forward Control

Another way to control ambient noise is to use feed-forward control. The microphone which is used to pick up the noise is placed outside on the casing of the headphone ear-cup. The feed forward control filter has to simulate the complex pressure relation between outside of the headphones and inside (where noise cancellation is desired). Feed forward loop shaping is very common in reducing broadband noise but has one of its limits due the directional dependency of sound sources [Gul14]. Different source angles and especially diffuse sound fields introduce incoherent phase relations between inside and outside the headphones and therefore make it harder to cancel out the unwanted signal.

1.4 Filter Optimization

Another vast field in research is the optimization of filters. Depending on the later use, different approaches for the filter design are possible to choose. In the active noise control theory, common approaches are the H_∞ and H_2 approaches, cf. [Zam81, FZ84, RE99]. The main target is to synthesize a controller for best performance and still guarantee stability. The classic approaches need a translation of a real dynamical system into a mathematical model. Typically, the plant model is defined in the state-space domain, although model matching is also a common practice [FZ84]. Since this design task is not an easy one, further investigations on approaches using data from impulse response measurements have been made. An approach in the cepstral domain formulated as a linear optimization problem and a nonlinear non-convex filter design technique in the complex domain will be examined in Sec. 3.4 and 3.5. Especially these newer types of active noise control filter optimization are interesting due to their intuitive use of raw measurement data

to represent the plant. Furthermore, the plant uncertainty of an ANC headphone can be described with additional sets of measurement data.

1.5 Motivation

There are several constraints and subjects necessary to fulfill to yield a stable optimal noise reduction system. Manual filter design for noise control systems is still an applied technique, because of its intuitiveness. A computer-aided feedback filter optimization can reduce the time consumption of the manually process and include plant uncertainties to guarantee stability. This thesis will focus on feedback ANC and the optimization of the feedback control filter for an analog design.

Chapter 2

Feedback ANC

The noise control and shaping of the closed loop system will be described thoroughly in this chapter. It is shown how a feedback loop is defined mechanically and how we can represent it mathematically. We will see how transfer functions can be used to describe the input/output relations of parts of the closed loop system and also how the tranfer function of the whole system can be denoted. Furthermore, it is shown how we can use this knowledge of the feedback-loop properties to control it and design a stable feedback loop.

2.1 Schematic Representation of a Feedback System

Figure 2.1 shows the mechanical representation of a feedback system as in common noise control headphones. The size of the headphone ear-cups can differ in commercial active noise control headphones. Some build a total enclosure around the ears, but there are also smaller types with ear-pads in the size of the pinna available. They also differ in their mechanical constitution, which depends on the materials used. A robust casing and a fixed microphone position in regard of the distance from the loudspeaker can improve the performance of a noise control headphone drastically. Many problems in terms of stability occur with the uncertainty of the mechanical system. An apparently stable system can become unstable immediately if mechanical deformation changes the overall system. One way of positioning a small microphone could be on the inside of the ear-cup in front of the loudspeaker

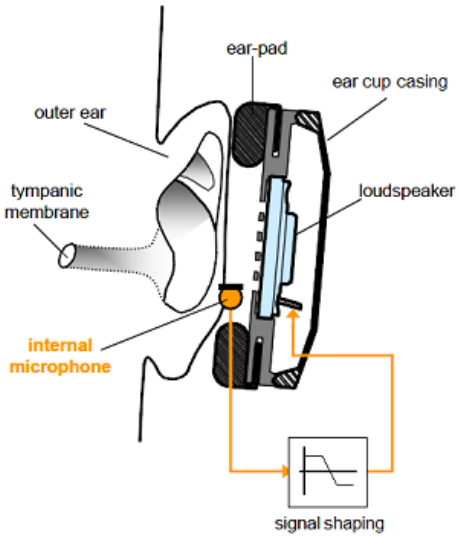

Figure 2.1: Schematics of a feedback system of conventional noise control headphones. The noise is picked up by the microphone and shaped by a filter to produce an anti-noise which is fed back to the loudspeaker [wm10].

and ear canal, respectively. The advantage is that the microphone picks up the sound signal with the almost identical phase information that will reach the ear and therefore a proper noise cancellation can be provided.

In [GMK05] investigations on how to position the microphones inside of the cups are made. It is shown that different positions yield different good results in terms of noise control and stability. The overall stability margins are dependent on the inherent frequency responses from the loudspeaker to the microphone, respectively. This transfer function forms the secondary path. The influence of the mechanical deformation and changes in the acoustics of the headphones onto the secondary path will be discussed in chapter 4.

The simplified mechanical representation of an ANC system is depicted in Fig. 2.2. The primary source introduces disturbances from the outside. The secondary source is the loudspeaker of the headphones. The microphone picks up the penetrating ambient noise and the played back anti-noise from the secondary source. The picked up signal is called the residual error signal, which is then shaped by an electrical filter to produce the control signal u. In Fig. 2.3 we see the block

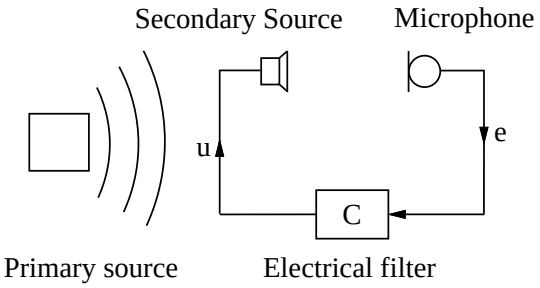

Figure 2.2: Schematics of an ANC feedback system with two sources. The primary source introduces disturbances, whereas the secondary source (i.e. the headphones loudspeaker) plays back the anti-noise. The residual error signal is described as e and the control (shaped) signal as u.

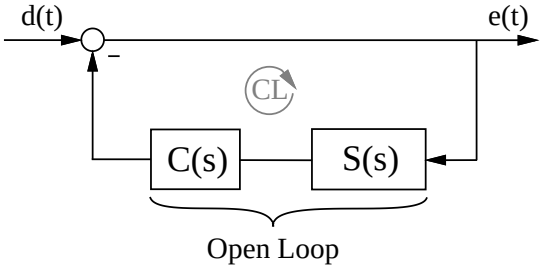

Figure 2.3: The combination of the transfer functions from the loudspeaker to the microphone and filter form the open-loop transfer function $L(s)$.

diagram of a classic noise-canceling feedback system. The Laplace-domain transfer function from the microphone to the loudspeaker is the plant, which is typically denoted as the secondary path $S(s)$ in active noise control. The filter to shape the signal is depicted as the block $C(s)$ and $d(t)$ is the disturbance signal and $e(t)$ the residual error signal. The description of the system in the Laplace-domain can be treated as in Eq. (2.1).

$$\begin{aligned} E(s) &= D(s) - E(s)S(s)C(s) \\ D(s) &= E(s) + S(s)C(s)E(s) = E(s)(\,1 + S(s)C(s)\,) \\ \frac{E(s)}{D(s)} &= \frac{1}{1 + C(s)S(s)} \end{aligned} \tag{2.1}$$

After the mathematical conversion, we yield the error output over the disturbance, which is called the sensitivity function of the closed loop. The closed loop magnitude

response of the output error in regard to the input signal holds information on how good noise reduction in each frequency band can be achieved [DFT91]. Eq. (2.2) represents the sensitivity function

$$\xi(s) = \frac{1}{1 + C(s)S(s)} = \frac{1}{|1 + L(s)|}, \tag{2.2}$$

and in dB

$$\xi(s)_{\mathrm{dB}} = 20 \log \frac{1}{|1 + L(s)|}, \tag{2.3}$$

where the transfer function $L(s) = C(s)S(s)$ is known as the open-loop transfer function (see Fig. 2.3). We want $L(s)$ to be as large as possible to minimize the sensitivity function, which equals a good noise rejection. This is only possible as long as the phase of $L(s)$ does not turn to -180°. This limits ANC to the low frequency region. However, minimzing the function in one frequency band leads to an amplification in another frequency band. If the phase value of the complex pointer $L(s)$ gets close to -π a constructive superposition will occur, which then amplifies the noise signal. This will be discussed in more detail in Sec. 2.2.3. Furthermore, the feedback loop bears the risk of instability (detailed description follows in Sec. 2.2.2, Fig. 2.6). If the phase value of $L(s)$ is at -π and the magnitude of $L(s)$ is larger than one, the feedback loop will become unstable. An example of the sensitivity function for a stable ANC system is depicted in Fig. 2.4.

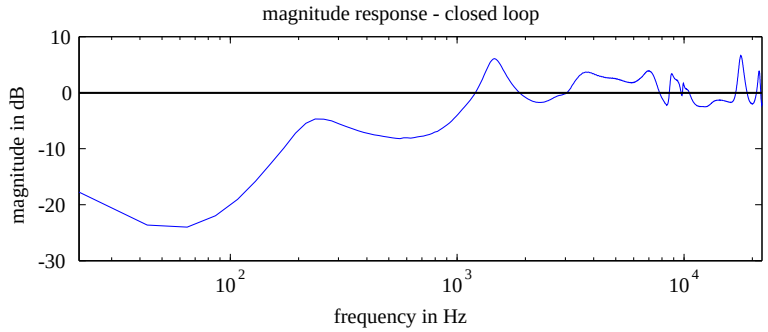

Figure 2.4: Closed loop magnitude response of an ANC system. The areas below unity depict the regions where noise cancellation is performed and the areas above unity depict noise amplification.

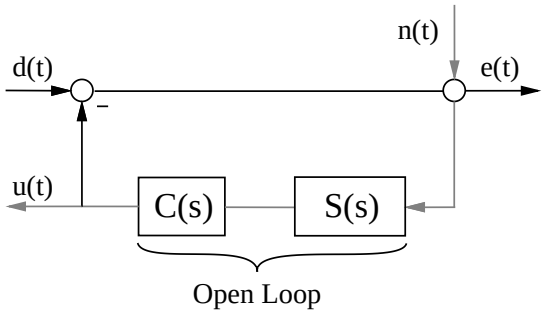

Figure 2.5: Block diagram of the closed loop feedback system. The grey lines depict the path for the definition of the output/input relation of the complementary sensitivity function, which gives information about the tracking performance of a control system. The input n(t) denotes sensor noise, which can occur at the microphone.

2.2 Transfer Functions

There are transfer functions of a feedback system that can be referred to as basics of control theory. The first one was already described as the *sensitivity function* and the second is denoted as the *complementary sensitivity function* in Eq. (2.4) and denotes the relation of the control signal and the measurement noise n as in Fig. 2.5[1].

$$T(s) = \frac{L(s)}{1 + L(s)} = \frac{U(s)}{N(s)}, \tag{2.4}$$

where $U(s)$ and $N(s)$ are the Laplace transform of the control signal u(t) and the measurement noise n(t), respectively. A block diagram of the output/input relation is depicted in Fig. 2.5.

A fundamental equation that connects these two closed-loop transfer functions is denoted in Eq. (2.5).

$$\xi(s) + T(s) = 1 \tag{2.5}$$

The two transfer functions share the same polynomials in the denominator. Therefore, we will have a closer look at the denominator of $T(s)$ and $\xi(s)$ in Eq. (2.6),

[1]There are further transfer functions for the overall system that give valuable informations about the system properties and are used in classic control theory, but will not discussed here [ÅM07].

respectively.

$$L(s) = \frac{\mu(s)}{\nu(s)} \qquad \text{and} \qquad 1 + L(s) = \frac{\mu(s) + \nu(s)}{\nu(s)}. \tag{2.6}$$

The polynomials of $\xi(s)$ follow to

$$\xi(s) = \frac{\nu(s)}{\mu(s) + \nu(s)}. \tag{2.7}$$

It can be seen that the denominator of $\xi(s)$ depends not only on the zeros but also of the poles of the open loop. Furthermore for a stable open loop, all the poles of $L(s)$ except for one on the imaginary axis and also all the zeros have to lie in the left half plane [HD06]. This relations allow us to state that the overall system is stable, if the continuous angle change of 1+L(s) is

$$\Delta \text{arc}\{1 + L(j\omega)\} = 0 \qquad \text{for } \omega \in [0, \infty). \tag{2.8}$$

Under the realistic assumption that the control filter and the secondary path are stable, the specific Nyquist criterion states that the closed loop is stable if the root locus of $L(s)$ does not encircle the point -1 in the complex plane, which gives us a nice relation between the properties of $L(s)$ and the stability of $\xi(s)$.

If we can shape $L(s)$ with the filter $C(s)$ in a manner that it fulfills the Nyquist stability criterion, stability for the closed system can be guaranteed.

2.2.1 Stability Constraints

As stated above, the robust stability of a closed-loop system can be fully determined via specific constraints of the open loop system. Per defintion a robust controller $C(s)$ provides robustness of the open loop for every secondary path $S(s)$ from a set of secondary paths $\mathcal{S}$. The phase margin, the gain margin and the root locus of the open loop transfer function give full information if the closed loop can reach a stable state. Further informations about the stability of the closed loop and the filter can be observed via the impulse response. In classic control theory literature, we will find the stability conditions defined via the Nyquist stability criterion which is a sufficient and necessary condition for stability. If only the phase and magnitude margins of the open loop are evaluated, but not the pole and zero locations of the transfer functions (cf. [HD06]), we can only fulfill sufficient, but not necessary conditions.

2.2.2 Phase Margin and Gain Margin

As one of the most critical constraints in feedback filter design we have the phase margin PM. The phase response of the open loop has to be within the region of π and $-\pi$ for the whole frequency band where the magnitude is above unity.

At the frequency where the magnitude of the open loop drops below the 0dB mark (at ω_c), the phase is allowed to have lower values than -π. The phase margin can be denoted as

$$\phi_m = \pi + arc\left\{L(j\omega_c)\right\}, \qquad \text{for } |L(j\omega_c)| = 1. \tag{2.9}$$

As mentioned, the phase margin in real environments has to be chosen rather conservative to prevent excessive noise amplification. Usually, a phase margin of 40° is denoted.

The second most critical constraint is the gain margin GM which is closely related to the phase margin PM. The gain in the frequency band of the open loop where noise reduction is performed (i.e. below approx. 1kHz[2]) should be positive. If the phase of the open loop reaches $-\pi$ the magnitude should be below unity to prevent noise amplification.

The magnitude of the open-loop where the phase becomes -π (at ω_0) is called the gain margin GM (Eq. 2.10).

$$GM\,|_{\text{dB}} = -20\log_{10}|L(j\omega_0)| \tag{2.10}$$

If these two constraints are chosen properly and controlled over the whole frequency range, we can prevent that the frequency response locus of the open loop $L(s)$ encircles the critical point -1.

[2]Due to a phase lag in real systems that can not be compensated.

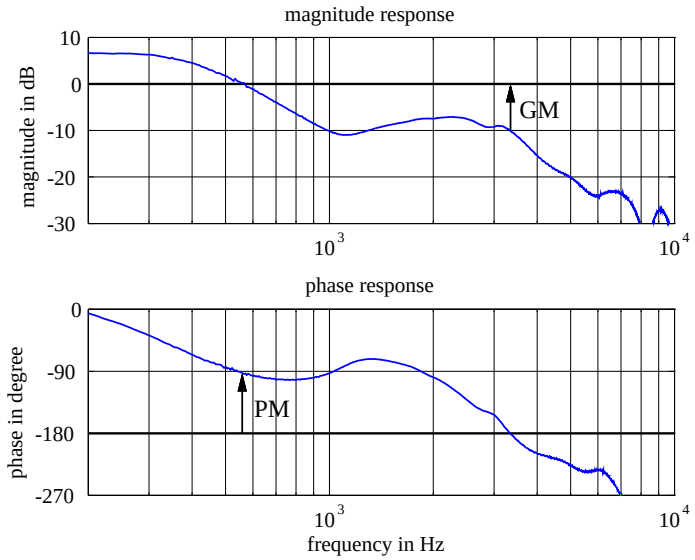

Figure 2.6: Gain margin GM and phase margin PM of an open loop in the Bode plot.

2.2.3 Waterbed Effect

If we try to minimize the sensitivity function over the whole frequency range, the waterbed effect is a problem which is typically encountered (see Fig. 2.7). Minimizing the sensitivity function in one frequency band can lead to an amplification somewhere in the rest of the magnitude spectrum. In specific we can define the term disturbance attenuation for $|\xi(j\omega)| < 1$ and disturbance amplification for $|\xi(j\omega)| > 1$. Furthermore, we can state that if the open loop transfer function has at least two more poles than zeros and the filter and secondary path form stable rational strictly proper functions, Eq. (2.11) is true for the closed-loop [ZWQ12, DFT91, Paw02].

$$\int_0^{+\infty} 20 \log_{10} |\xi(j\omega)| \, d\omega = 0 \tag{2.11}$$

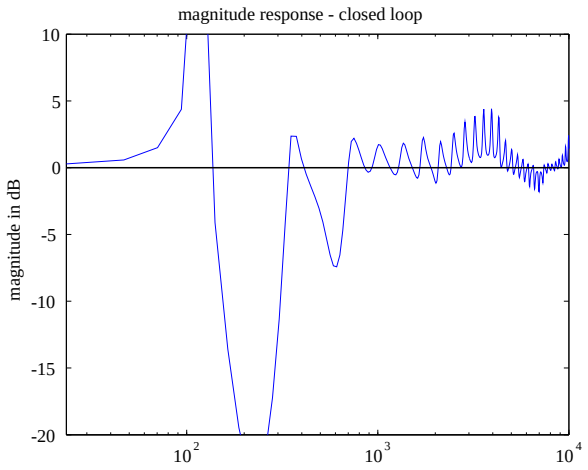

Figure 2.7: Example of the waterbed effect. We can distinguish between disturbance attenuation $|\xi(j\omega)| < 1$ and disturbance amplification $|\xi(j\omega)| > 1$.

2.2.4 Impulse Responses

The closed loop impulse response gives valuable information about the stability, on how much noise amplification is inherent and foremost how fast the system reaches a stable state. If the impulse response oscillates more than a few milliseconds the process of reaching a stable state will be audible. The oscillation needs to decay over time and has to converge to zero. In Fig. 2.8 we see impulse responses for three different cases. We can distinguish between a system that is stable and has a low decay time, a system which needs more time to reach a stable state and a unstable system.

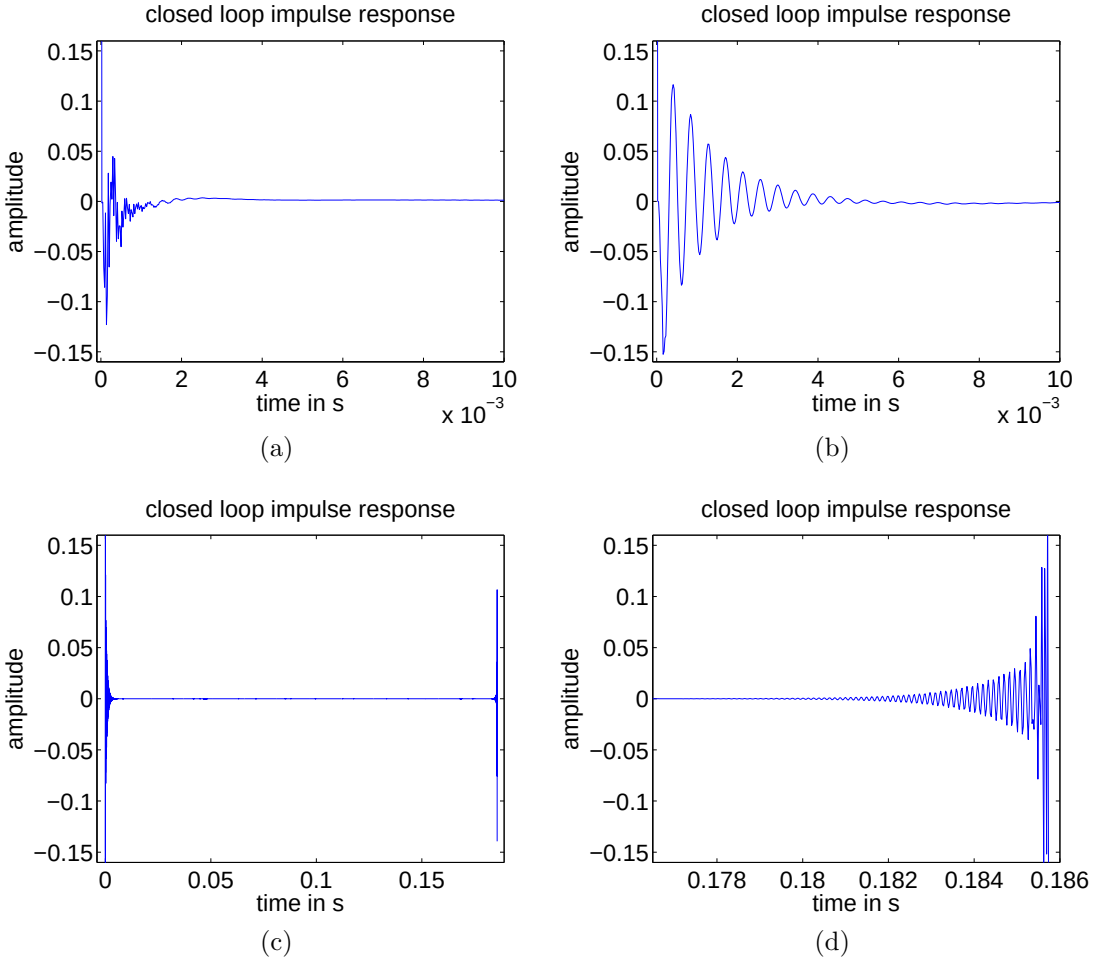

Figure 2.8: Closed loop impulse responses for different scenarios. a) depicts a stable system impulse response, b) also stable, but a higher overshoot and therefore a longer decay time c) acausality: the impulse response indicates an acausal system, which can by seen by the circular shift of the acausal part to the end of the impulse response due to the periodic property of the discrete Fourier transform. d) zoom on the acausal part in c).

Chapter 3

ANC Filter Design

A classic approach of analog filter design for active noise control headphones is to use a shelving filter or the combination of peak/notch filters to achieve an amplification of the open loop gain in the lower frequency band and an attenuation in the high frequency range to yield a low pass characteristic and therefore a stable transfer function. The concept is also useful in regard of the phase design, because the mentioned filters have manageable phase responses for lower orders and do not tend to overstep the phase margin too fast (i.e. the stability bound of the phase response $-\pi$ and $+\pi$).

If an optimal filter for a stable closed loop is demanded, optimization tools come in handy to consider several design criterion. As stated in the preceding chapter, we need to consider the waterbed effect. Furthermore we can state that the human auditory system does not have a constant sensitivity for all frequencies. This is shown by the Fletcher-Munson curves (i.e. equal-loudness contour). The human ear is most sensitive between 2 and 5kHz and less sensitive above and below.

3.1 Hearing Model

Due to the fact that the auditory system is less sensitive at low frequencies, we should not emphasize too much on that frequency region. Typically, the ear-cups of a closed headphone system damp ambient noise in the high frequency region. This damping can be represented with the magnitude response of a 2nd order low pass [GH13]. The sensitivity in the high and low frequency region can be represented as

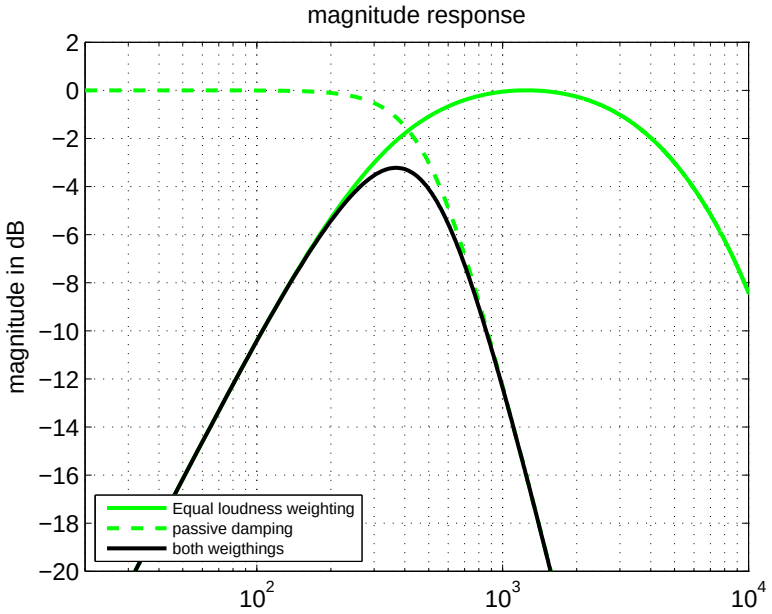

Figure 3.1: Weighting functions for the ANC performance in regard of the sensitivity of the auditory system. The dashed line indicates the passive damping of higher frequencies of the ear-cup which can be measured for each headphone. The solid line represents the behavior of the human auditory system with less sensitivity for very low and high frequencies. The ANC performance should therefore be weighted with the combination of the two weighting functions (solid black).

a 1st order bandpass. Under these two assumptions we can set up a performance analysis of the closed loop system which includes the behavior of the auditory system and the damping of the ear-cups. In Fig. 3.1 we use a magnitude response of a 2nd order low pass with a cut-off frequency at 500Hz to represent the damping of the headphones. We can also measure the passive low pass damping for each type of headphones. A 1st order bandpass with a lower cut-off frequency at 300Hz and an upper cut-off frequency of 5kHz represents the lack of sensitivity for very low and high frequencies of the auditory system. It is also a common method to include the A-weighting in the optimization procedure [HP09].

3.2 State of the Art Manual Filter Design

3.2.1 Shelving Filter

In this section, the classic approach to design a filter to form a stable closed loop is described. Starting with a transfer function from raw measurement data depicted in Fig. 3.2, we can use a standard low-shelv filter to increase the open loop gain in the low frequency region and attenuate the magnitude in the high frequency region. The design criterion is that the open loop for $|L(j\omega)| = 1$ still has a phase higher than -π.

In most commercial products, the noise amplification margin for $\xi(s)$ is around 4dB. This constraint has two degrees of freedom, namely the magnitude and phase of the open loop. We now demand as an example a phase margin PM of 40°. This means that the maximum open loop gain α can be calculated over

$$20 \log \left| \frac{1}{1 + \alpha e^{-j\frac{7\pi}{9}}} \right| \leqslant 4\text{dB}. \tag{3.1}$$

3.2.2 Peak/Notch Filter Combination

A combination of a peak and notch filter is another way to treat the problem of manually designing a stable open loop. The peak filter is used for the amplification in the frequency region below 1kHz and the notch filter is used for raising the phase in the higher frequency range to gain better overall performance. The combination of these filter types is nothing more than the multiplication of the two in the frequency domain cf. Fig. 3.3 (or a convolution in the time domain). The same margins for the design are valid as in Sec. 3.2.1. The advantage of this design is the possibility to yield a higher noise reduction in a specific frequency band and due to the behavior of the phase response of this filter a notch filter is used to increase the phase for higher frequencies to stabilize the open loop over a broader frequency range, cf. Fig. 3.4.

The techniques presented in the two preceding subsections introduced the manual controller design for a feedback loop, which is also referred to as loop shaping. The idea is to find a rational strictly proper transfer function L(s) which fulfills the gain and phase margin. One can imagine that an optimal design via

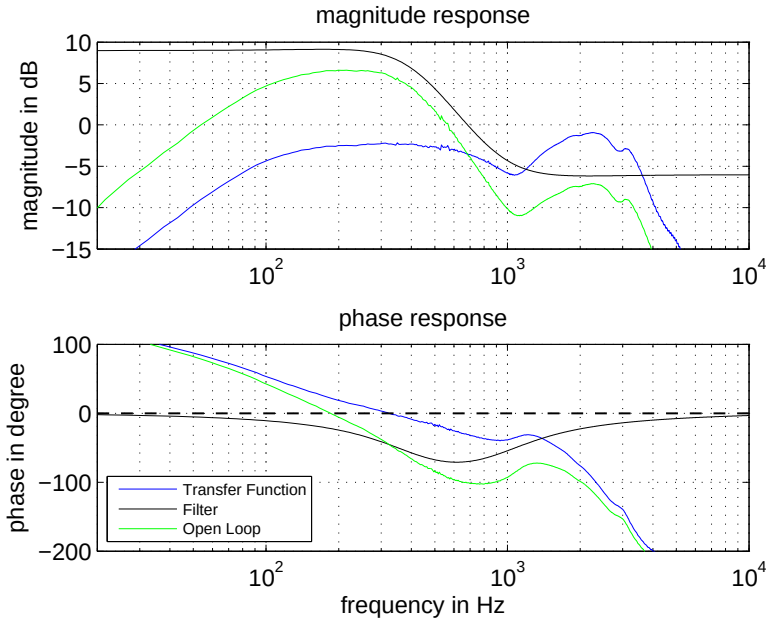

(a) Bodediagram

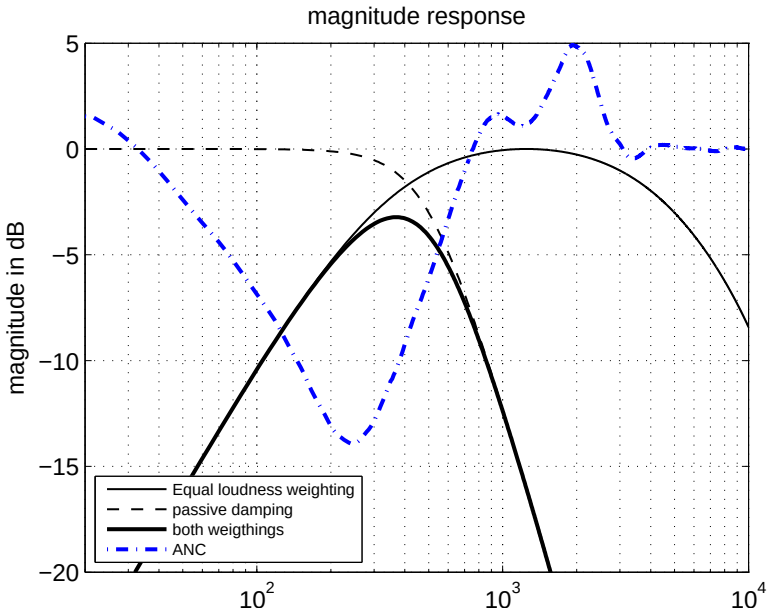

(b) ANC-Performance Analysis

Figure 3.2: Manually loop shaping of a secondary path a) depicts the open-loop and the used low-shelv filter, b) depicts the performance analysis diagram of the design.

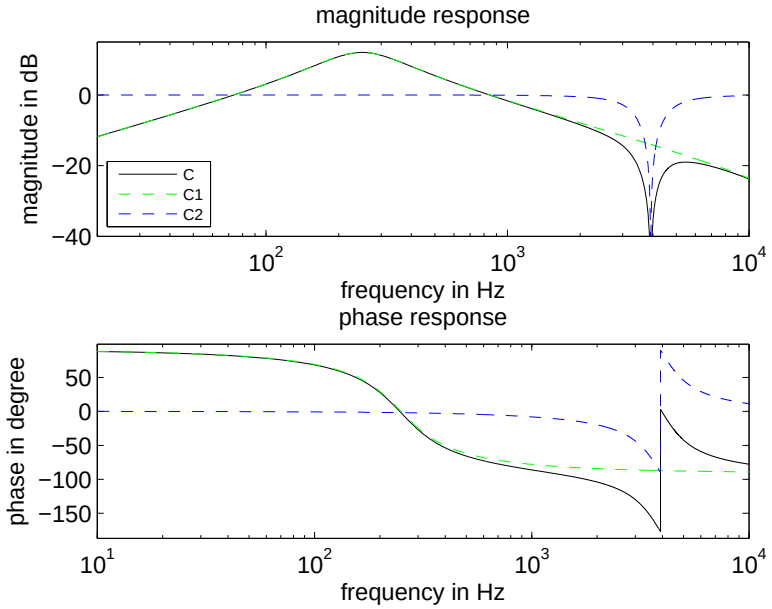

Figure 3.3: Frequency response of the two filter types for loop shaping with the peak/notch combination denoted as C1 (peak filter) and C2 (notch filter) and the overall frequency response.

manually shaping is nearly impossible and that is why automated optimization techniques for feedback control are vastly investigated in scientific research [FK95].

3.3 H_2/H_∞ Optimization

The manual filter design for the open loop shaping is quite intuitive if the necessary criteria are known. The disadvantage is that every plant needs its own filter tuning and inevitably leads to a large time consumption. In the case of filter design for active noise control headphones the misuse scenarios (i.e different wearing characteristics or behaviors of the user) are building a set of plants which need to be considered in the design task of the optimal filter. But for now we emphasize on the optimal design for one specific secondary path as a linear or even non-linear programming problem. As indicated in the introduction the H_2 and H_∞ approaches are well studied in literature and practice. Therefore these two will be investigated in the following sections.

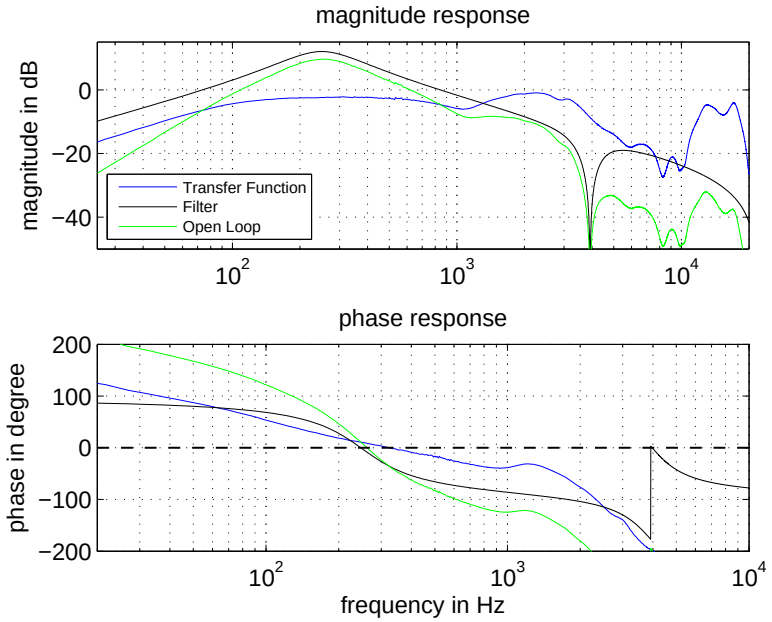

(a) Bodediagram

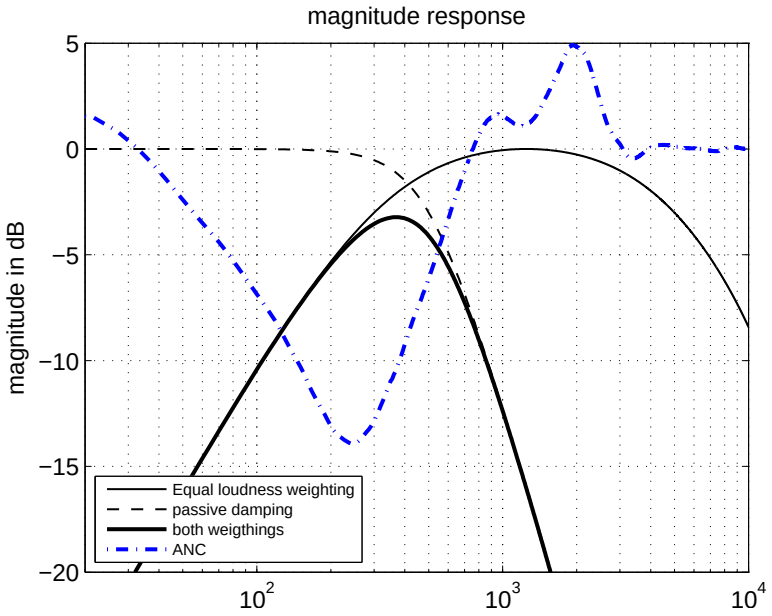

(b) ANC-Performance Analysis

Figure 3.4: Manual loop shaping of a secondary path a) depicts the open-loop and the used peak/notch filter, b) depicts the performance analysis diagram of the design.

3.3.1 H_2/H_∞ Norm and Weighting Functions

In classic control theory, we investigate the stability of a rational transfer function by its pole constellation. If the degree of the polynomial of the numerator is less than the degree of the denominator the function is strictly proper. If the degree is the same, the function is called proper. For all physical dynamical systems, a roll-off behavior for high frequencies is inherent (i.e. low pass characteristic) and therefore they have a strictly proper transfer function.

In regard of optimizing the sensitivity function (i.e. shaping and optimizing the output of the feedback loop) two norms are introduced. The H_2 norm Eq. (3.2) and the H_∞ norm[1] Eq. (3.3) are useful tools to minimize the energy or the amplitude of the sensitivity function in the latter case.

$$\|\xi\|_2 = \left[\frac{1}{2\pi}\int_{-\infty}^{\infty} |\xi(j\omega)|^2 \, d\omega\right]^{1/2}, \tag{3.2}$$

$$\|\xi\|_\infty = \sup_\omega \sigma_{max} |\xi(j\omega)| \qquad (\sigma_{max} := \text{maximum singular value}) \tag{3.3}$$

As already described in Sec. 2.2.3, the sum of the area above and below unity of $|\xi(j\omega)|$ over the whole frequency range is zero. If we now want to minimize the overall function, we won't yield a maximization of the noise reduction in the low frequency range as it is requested in active noise control. It is necessary to emphasize on the region of interest (i.e. the region where the magnitude of the sensitivity function should become as minimal as possible) with a weighting function.

In control theory there are typically three weigthing functions used to shape the feedback loop. Typical the sensitivity function, the complementary sensitivity function and the controller are weighted with W_S, W_T and W_C. The controller weight W_C is used toe emphasize on the frequencies in the control signal where most of the energy lies. The weight W_S can be chosen, such that W_S^{-1} reflects the desired shape of the sensitivity function. Low gain at low frequencies yield in a good tracking performance and high gain in the high frequency region limits the overshoot.

[1]For the sake of completness it should be denoted that the H norms are Hardy spaces which are specially defined subsets of L^p spaces for strictly proper functions [FZ84, Zam81].

3.3.2 System Model and Constraints in the State Space Domain

H_2 and H_∞ loop shaping demand a system representation in the state-space domain. The state-space model describes linear system equations in matrix notation. Each matrix holds valuable information about the states and the abilities of the system such as controllability and observability cf. Eq. (3.4) [HD06].

$$\begin{aligned} \frac{d\mathbf{x}}{dt} &= \mathbf{A}\mathbf{x} + \mathbf{b}u \\ y &= \mathbf{c}^T\mathbf{x} + du \end{aligned} \tag{3.4}$$

The variables [$\mathbf{A}, \mathbf{b}, \mathbf{c}$,$d$] are constant and represent the system. The state vector $\mathbf{x}$ holds information about the internal system variables. Under compliance of certain constraints on the vectors $\mathbf{b}$, $\mathbf{c}$ and $\mathbf{A}$ in the state-space domain, a stable controllable and/or observable system can be formed. Furthermore, constraints can be set to force certain performance issues as command tracking or disturbance rejection. One constraint in terms of stability is that the characteristic polynomial $\Delta_n(s)$ of the matrix $\mathbf{A}$ is a Hurwitz polynomial cf. Eq. (3.5).

$$\Delta_n(s) = a_n s^n + a_{n-1} s^{n-1} + ... + a_1 s + a_0 \tag{3.5}$$

All the real zeros of $\Delta_n(s)$ have to be negative, or in case of complex zeros, the real part has to be negative. The sensitivity function, which shall be minimized can be expressed with the state-space representation as

$$\|\xi(s)\|_2 := \left\| \frac{y(s)}{u(s)} \right\|_2 = \left\| \mathbf{c}(sI - \mathbf{A})^{-1}\mathbf{b} \right\|_2, \tag{3.6}$$

where $\mathbf{d}$ equals zero in this case due to the prerequisite that the system is strictly proper.

3.3.3 Deriving a State Space Model

The task of defining a mathematical model of a dynamic system is not a trivial one. Usually only very simplified models of real physical systems are available. In contrast, it is easy and typical to identify a system via an impulse response measurement. The result of the measurement (i.e. an impulse response) can be Fourier transformed from the time domain to the frequency domain to analyse the systems behavior. The complex valued spectrum achieved via the transformation can be modeled with poles and zeros, which yield a rational transfer function

$$H(s) = \frac{B(s)}{A(s)} = \frac{b_0 s^{n-1} + b_1 s^{n-2} + ... + b_{n-1} s + b_n}{s^n + a_1 s^{n-1} + ... + a_{n-1} s + a_n}, \tag{3.7}$$

with the degree of the numerator smaller as the denominator (strictly proper). This rational transfer function can't be easily obtained from the frequency response data. We need to do an approximation of the data, which is possible with a algorithm that minimizes the error of the data and the fractional approximate in form of

$$\min \sum_{k=1}^{N} \left| A(j\omega_k) H(j\omega_k) - B(j\omega_k) \right|, \tag{3.8}$$

or

$$\min \sum_{k=1}^{N} \left| \frac{B(j\omega_k)}{A(j\omega_k)} - H(j\omega_k) \right|^2, \tag{3.9}$$

where the latter one can be calculated via an interative search algorithm [SM65]. The result of the approximation can be improved for low frequencies by using a weighting function on the minimized error.

Fig. 3.5 depicts a comparison of the algorithms for complex curve fitting implemented in the technical computing language software Matlab. After the modeling of the transfer function the coefficients can be easily used to describe the system in the state-space representation. This can be done by using the controllable or observable cannonical form due to the properties of the dynamical system (strictly proper)[HD06]. We can take the coefficients from Eq. (3.7) and insert them like denoted in Eq. (3.10) and (3.11), which is the controllable canonical

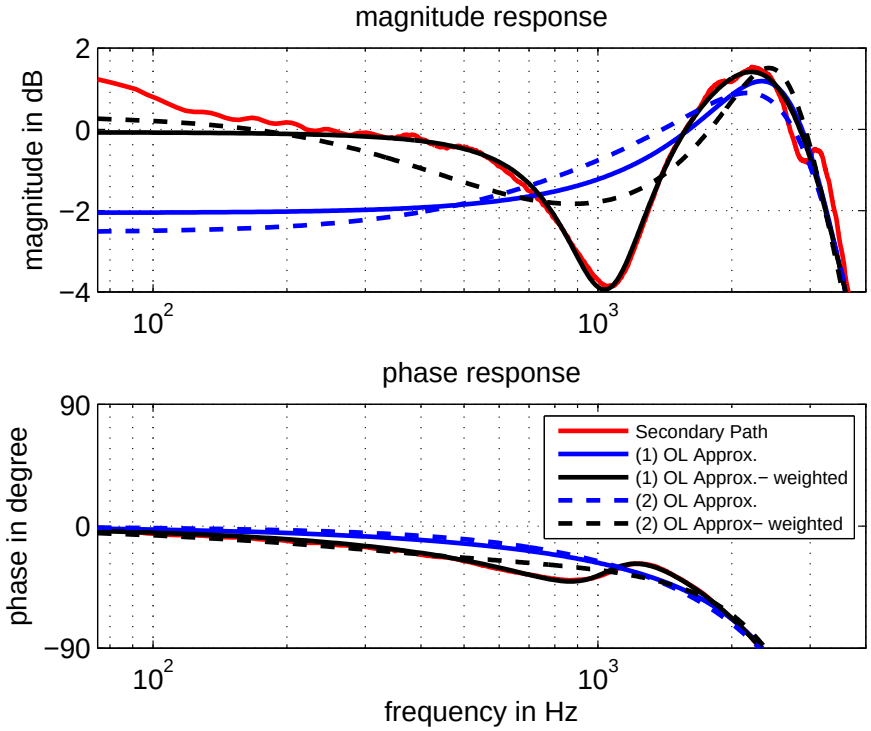

Figure 3.5: Comparison of the implemented curve fitting algorithms in Matlab. Algorithm (1) is the iterative approach from Eq. (3.9), which yields the best result if higher weights are used on low frequencies (black solid bold line). The results of algorithm (2) described in Eq. (3.8) differ especially in the low frequency region from the original transfer function. Both algorithms were used for a 10^{th} order transfer function approximation.

form of a state space model[2].

$$\frac{d\mathbf{x}}{dt} = \begin{pmatrix} 0 & 1 & . & 0 & 0 \\ 0 & 0 & . & 1 & 0 \\ . & . & . & . & . \\ 0 & 0 & . & 0 & 1 \\ -a_n & -a_{n-1} & . & -a_2 & -a_1 \end{pmatrix} \mathbf{x} + \begin{pmatrix} 0 \\ 0 \\ . \\ 0 \\ 1 \end{pmatrix} u \tag{3.10}$$

$$y = \begin{pmatrix} b_n & b_{n-1} & . & b_1 & b_0 \end{pmatrix} \mathbf{x} + 0u \tag{3.11}$$

There is already an implementation of such a transformation procedure in Matlab and of course an optimization tool to calculate the H_∞ optimization. Nevertheless, the modeling of the transfer function and choosing proper weighting functions for the optimization is not an intuitive task. That is why two more approaches will be presented in the next sections, which only require a simple impulse response measurement of the secondary path S, without further modeling.

3.4 Linear Optimization in the Cepstral Domain

The design technique [Lar07] described in this section emphasizes on maximizing the noise rejection via a classic set of constraints known from filter design and loop shaping to guarantee closed-loop stability. The approach is designed to use frequency response data from impulse response measurements instead of a plant model. The phase and gain margin for stability can be set as open-loop constraints in the cepstral domain and form a linear optimization problem. The cepstrum is commonly used to analyze speech in signal processing and is defined as the inverse Fourier transform of the logarithm of a spectrum. Known terms in the frequency domain like frequency, spectrum, filtering and harmonics are reversed by their first four letters to form the cepstral terms quefrency, cepstrum, liftering and rhamonics.

3.4.1 Complex Cepstrum Decomposition

The complex cepstrum $\hat{x}$ of a discrete signal $x(n)$ is defined as follows

$$X(e^{j\omega}) = \sum_{-\infty}^{\infty} x(n) e^{-j\omega n} \tag{3.12}$$

[2]A proper system can also be transformed, but has to be split up into a strictly proper part and a constant part [Wik14].

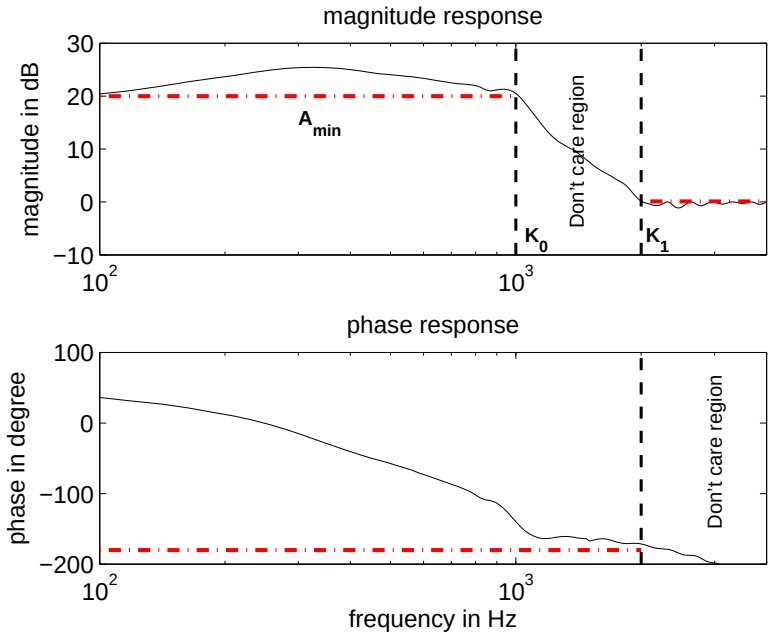

Figure 3.6: Design template for the open loop. Below K_0 the magnitude is maximized and above K_1 the magnitude is restricted to stay below 0dB. The phase constraints prohibits that the phase of the open loop takes the value equal to or below -π for frequency bins below K_1.

$$\log[X(e^{j\omega})] = \log\left|X(e^{j\omega})\right| + j\angle X(e^{j\omega}) \tag{3.13}$$

$$\hat{x}(n) = \frac{1}{2\pi}\int_{-\pi}^{\pi} \log[X(e^{j\omega})]e^{j\omega n}d\omega, \tag{3.14}$$

where Eq. (3.12) describes the time discrete Fourier transform, (3.13) defines the complex logarithm and (3.14) derives the cepstral coefficients.

3.4.2 Optimization and Constraints on the Open Loop

The goal of the optimization approach by [Lar07] is to maximize the open loop gain in the low frequency band up to frequency bin K_0, as in Fig. 3.6. The region between K_0 and K_1 allows the open loop to roll off. Above this "don't care" region, the magnitude is constrained to stay below 0dB. This constraint together with the restriction that the phase is not allowed to reach -π for frequencies below K_1 guarantees stability for the defined frequency range of the open loop. As a design

criteria, we can attest in terms of stability that a minimum-phase filter will yield the same or even better result than a nonminimum-phase filter. If we request a resulting digital filter C(z) to be minimum-phase the cepstrum is causal and therefore negative time indices can be omitted [OS89].

$$\sum_{n=0}^{N} \hat{c}(n) e^{-j\omega n} = \log(C(e^{j\omega})) = \log \left| C(e^{j\omega}) \right| + j \angle C(e^{j\omega}). \tag{3.15}$$

For defining the constraints we can transform the open loop to the cepstral domain and split up the phase and magnitude term with the even and odd part of the Fourier transform (cf. Eq. (3.15) in the following way

$$\begin{aligned} \log(C(e^{j\omega})) &= \sum_{n=0}^{N} \hat{c}(n) \cos(\omega n) - j \sum_{n=0}^{N} \hat{c}(n) \sin(\omega n) \\ \log \left| S(e^{j\omega}) C(e^{j\omega}) \right| &= \log \left| S(e^{j\omega}) \right| + \sum_{n=0}^{N} \hat{c}(n) \cos(\omega n) \\ \angle [S(e^{j\omega}) C(e^{j\omega})] &= \angle S(e^{j\omega}) - \sum_{n=0}^{N} \hat{c}(n) \sin(\omega n). \end{aligned} \tag{3.16}$$

The formulation shows that the magnitude and phase components can be expressed as a linear combination. A limited number of causal (n>0) cepstral coefficients M are defined to approximate the system[3]. We now want to define a linear optimization problem for that the open loop gain is maximized in the defined frequency region. Therefore, [Lar07] defines a variable A_{min} that represents the minimum open loop gain below K_0.

With this, [Lar07] defines a vector $\mathbf{x}$ which holds the variable A_{min} and the real cepstral coefficients $\hat{c}(n)$

$$\mathbf{x} = (A_{min}, \hat{c}(0), \hat{c}(1), ..., \hat{c}(M-1))^T. \tag{3.17}$$

[3]There is no need to make M too large, because in this approach we seek for the energy in the signal, which is due to the properties of the cepstrum in the lower quefrencies and the harmonics of a frequency response lie at higher quefrencies.

The first constraint that is introduced ensures that the magnitude of $L(s)$ stays above A_{min} in the frequency region up to K_0:

$$\begin{aligned}
&\mathbf{B_{pass}} \cdot \mathbf{x} < \mathbf{c_{pass}} \text{ with} \\
&\mathbf{B_{pass}} = \begin{pmatrix} 1 & -C_0^0 & -C_1^0 & ... & -C_{M-1}^0 \\ 1 & -C_0^1 & -C_1^1 & ... & -C_{M-1}^1 \\ . & . & . & ... & . \\ 1 & -C_0^{K_0} & -C_1^{K_0} & ... & -C_{M-1}^{K_0} \end{pmatrix} \\
&\mathbf{c_{pass}} = \begin{pmatrix} \log|S(\omega_0)| \\ \log|S(\omega_1)| \\ ... \\ \log|S(\omega_{K_0}| \end{pmatrix},
\end{aligned} \tag{3.18}$$

The angular frequency is defined as $\omega_k = 2\pi k/N$ for k=[0...$\frac{N}{2}$], N describes the number of frequency points, K_0 the upper frequency bin of the pass section and the sine and cosine functions of the summation terms in Eq. (3.16) are denoted as coefficients $C_n^k = \cos(\omega_k n)$ and $S_n^k = -\sin(\omega_k n)$.
For the stop section, we define

$$\begin{aligned}
&\mathbf{B_{stop}} \cdot \mathbf{x} < \mathbf{c_{stop}} \text{ with} \\
&\mathbf{B_{stop}} = \begin{pmatrix} 1 & C_0^{K_1} & C_1^{K_1} & ... & C_{M-1}^{K_1} \\ 1 & C_0^{K_1+1} & C_1^{K_1+1} & ... & C_{M-1}^{K_1+1} \\ . & . & . & ... & . \\ 1 & C_0^{K_{N/2-1}} & C_1^{K_{N/2-1}} & ... & C_{M-1}^{K_{N/2-1}} \end{pmatrix} \\
&\mathbf{c_{stop}} = \begin{pmatrix} -\log|S(\omega_{K_1})| \\ -\log|S(\omega_{K_1+1})| \\ ... \\ -\log\left|S(\omega_{K_{N/2-1}}\right| \end{pmatrix}
\end{aligned} \tag{3.19}$$

and for the phase restriction section we denote

$$\begin{aligned}
&\mathbf{B_{phase}} \cdot \mathbf{x} < \mathbf{c_{phase}} \text{ with} \\
&\mathbf{B_{phase}} = \begin{pmatrix} 0 & -S_0^0 & -S_1^0 & ... & -S_{M-1}^0 \\ 0 & -S_0^1 & -S_1^1 & ... & -S_{M-1}^1 \\ . & . & . & ... & . \\ 0 & -S_0^{K_1} & -S_1^{K_1} & ... & -S_{M-1}^{K_1} \end{pmatrix} \\
&\mathbf{c_{phase}} = \begin{pmatrix} \pi + \angle S(\omega_0) \\ \pi + \angle S(\omega_1) \\ ... \\ \pi + \angle S(\omega_{K_1}) \end{pmatrix}.
\end{aligned} \tag{3.20}$$

It is further possible to extend the constraints with more restrictions on the phase and gain margins to ensure stability and prevent excessive noise amplification for the closed loop.

3.4.3 Linear Optimization Problem

All constraints in matrix notation are put together in a large $\mathbf{B}$ matrix and all vectors are also connected to a vector $\mathbf{c}$. At last we define a vector $\mathbf{a}^T = (-1, 0, ..., 0)$ to complete the linear optimization problem of the form

$$\mathbf{a}^T \cdot \mathbf{x}, \text{ subject to constraints } \mathbf{B} \cdot \mathbf{x} < \mathbf{c}. \tag{3.21}$$

The problem can be solved via the *linprog* algorithm in Matlab and results in vector $\mathbf{x}$ with the cepstral coefficients of a causal minimum-phase filter, which can be then transferred to the time domain. A causal cepstrum corresponds always to a causal time domain signal. Therefore, the properties of the cepstrum allow the following recursion to calculate the filter's impulse response [OS89]

$$c(n) = \begin{cases} 0, & \text{for } n \leq 0 \\ \exp(\hat{c}(0)), & \text{for } n = 0 \\ \frac{1}{n} \sum_{k=0}^{N-1} k\hat{c}(k)c(n-k), & \text{for } n \geq 0. \end{cases}$$

3.4.4 Pros and Cons

A big advantage of the approach in the cepstral domain is that the constraints are in a linear relationship and therefore it is an easy calculation task for modern computers. The optimization results in a global minimum, which means in the optimal filter solution for a specific set of constraints. Nevertheless, the resulting filter impulse response is infinite and needs to be truncated at one point and transformed to a rational transfer function. Still, this optimal filter can be used as a design sheet for an analog filter design.

If we want to design an analog filter directly from the truncated impulse response, we can use an approximation algorithm like the proposed by [SM65]. The algorithm calculates coefficients for an IIR (infinite impulse repsonse) filter representation. The IIR filter is a recursive filter that allows us to describe an arbitrary long impulse response via a fractional recursion formula [OS89].

Another big advantage is that the approach emphasizes on the design of an ANC filter in terms of data from impulse response measurements. It also allows to consider more than one secondary path to constrain the filter optimization, which can lead to a design that guarantees stability for all possible misuse scenarios (more details in chapter 4).

3.5 Optimization for a Limited Order Filter

As another optimization approach the controller design technique from [SH01] is investigated. The optimization problem here is formulated as the minimization of the H_2 norm of $\xi(s)$, cf. Eq. (3.2), in the frequency domain and constraints are set as a nonlinear function in the complex plane. Furthermore, the filter order is explicitly specified which also leads to a non-convex minimization task.

3.5.1 Constrainted Optimization and Controller

We yield good results for the noise rejection, if we minimize the magnitude of the sensitivity function over a certain bandwidth. In terms of minimizing the outcome of the error to disturbance relation we have denoted the H_∞ and H_2 norm, whereas the latter one is employed as the measure for minimizing the average power of the unwanted noise signal. We can denote a weighted optimization problem, as

$$\min_{\mathbf{x}} \int_0^\infty \left| \frac{1}{1 + L(\mathbf{x}, \omega)} \right|^2 W(\omega) d\omega \qquad \forall \omega \in [0, \infty), \tag{3.22}$$

where $L(\mathbf{x}, \omega)$ is the open loop and $W(\omega)$ is a weighting function to define the frequency region where most of the noise disturbance is assumed or where the best ANC performance is demanded. The vector $\mathbf{x} = [\mathbf{a},\ \mathbf{b}] \in \mathbb{R}^{2n+1}$, holds the denominator and numerator coefficients of the nth-order controller We also want to restrict the optimization to yield a robust stable controller and that's why certain stability constraints have to be set for the controller and the open loop. For a stable closed loop, two conditions are necessary: 1) The IIR control filter has to have its poles in the left half plane. 2) The closed loop has to have its poles also in the left half plane.

3.5.2 Controller Stability

First of all, we expect the plant $S(j\omega)$ (i.e the secondary path) to be stable. This can be assumed due to the fact that every dynamic system can be described via a strictly proper transfer function which has a low pass behavior for high frequency

and a high pass behavior for very low frequencies. The controller is defined as

$$C(s) = \frac{b_0 s^n + b_1 s^{n-1} + .. + b_n}{s^n + a_1 s^{n-1} + .. + a_n}. \tag{3.23}$$

We can multiply the Eq. (3.23) by s^{-n}

$$C(s) = \frac{b_0 + b_1 s^{-1} + .. + b_n s^{-n}}{1 + a_1 s^{-1} + .. + a_n s^{-n}}. \tag{3.24}$$

With

$$\begin{aligned} \mathbf{a} &= \begin{bmatrix} 1 & a_1 & a_2 & ... & a_n \end{bmatrix}^T \\ \mathbf{b} &= \begin{bmatrix} b_0 & b_1 & b_2 & ... & b_n \end{bmatrix}^T \\ \mathbf{w} &= \begin{bmatrix} 1 & (j\omega)^{-1} & (j\omega)^{-2} & ... & (j\omega)^{-n} \end{bmatrix}^T, \end{aligned} \tag{3.25}$$

the filter can be denoted as

$$C(\mathbf{x}, \omega) = \frac{< \mathbf{b}, \mathbf{w} >}{< \mathbf{a}, \mathbf{w} >} \tag{3.26}$$

where the symbol ^{T} denotes the vector transpose and the operator $<,>$ the element-wise vector multiplication. The variable n specifies the order of the controller. To force stability for the controller we use the Lienard-Chipart criterion, which is a simplification of the Hurwitz criterion. All the poles of the transfer function of $C(\omega)$ must lie in the left half plane, [HD06]. This can be guaranteed, if the polynomial of the denominator (i.e. characteristical polynomial $\Delta_n(s)$ in Eq. (3.27)) of the controller $C(\omega)$ is a Hurwitz polynomial. The Lienard-Chipart criterion states that

$$\Delta_n(s) = a_0 s^n + a_1 s^{n-1} + ... + a_{n-1} s + a_n, \qquad \text{with } a_0 > 0 \tag{3.27}$$

is a Hurwitz polynomial, if one of the sequences

$$\{a_2 > 0, \quad a_4 > 0, \quad a_6 > 0, ... \quad a_n > 0\} \text{ or } \{a_1 > 0, \quad a_3 > 0, \quad a_5 > 0, ... \quad a_n > 0\}$$

and one of the sequences

$$\{D_1 > 0, \quad D_3 > 0, \quad D_5 > 0, ...\} \text{ or } \{D_2 > 0, \quad D_4 > 0, \quad D_6 > 0, ...\}$$

where D_k denotes the determinants of the Hurwitz matrix, hold exclusively elements with the same sign [HD06]. If true, it is no longer necessary to investigate the zero locations of the characteristical polynomial $\Delta_n(s)$.

3.5.3 Necessary and Sufficient Closed Loop Stability

After assuming stability of $C(s)$ and $L(s)$, respectively, we can now investigate the root locus of $L(s)$ in the complex plane to analyze the stability of the closed loop. The nyquist plot is used to visualize the behavior of the open loop over the whole frequency range. It can be stated that if $L(s)$ does not encircle the critical point -1, the closed loop stability is guaranteed[4]. For ensuring this criterion on a digital computer we need to define forbidden regions in the nyquist plot Fig. 3.7, because a direct translation is difficult and inefficient [Pol84].

The parabola in Fig. 3.7 forces the contour L(s) to stay on the right side of the point -1+0j. The parabola equation can be stated in Cartesian coordinates as

$$x = d_1 y^2 - d_2. \tag{3.28}$$

The constraint on $L(s)$ in the complex plane follows to

$$\Re\{L(\mathbf{x}, \omega)\} \geqslant -d_1 \, \Im\{L(\mathbf{x}, \omega)\}^2 - d_2, \tag{3.29}$$

where d_1 denotes the opening of the parabola and d_2 the distance from the vertex to the origin. With this we have not only set a necessary and sufficient stability bound, but also a bound in regards of the systems sensitivity for perturbation, which we can be denoted as the distance from the origin to the point where the parabola crosses the real axis. Due to typical discretization on a computing system, the number of frequency points used in the calculations should be large enough to ensure that the interpolation between two frequency points is still outside the "Forbidden Region 1".

Furthermore, can we prevent excessive noise amplification for the whole frequency range via the "Forbidden Region 2", which ensures that the absolute value of the complex pointer $L(s)$ does not get too large in the region where the $\arg\{L(s)\}$ is almost $-\pi$. This forbidden region is defined as the space inside a circle with the center at $\Re\{L(s)\} = -1$ and radius b (dash-dotted).

Another behavior we wish for the open loop is a low pass characteristic in the

[4]It shall be mentioned that an unstable open loop with P unstable poles needs N clockwise encirclements to result in a stable closed loop and following the equation Z=P+N=0, where Z is the number of real poles of the closed loop in the right half plane.

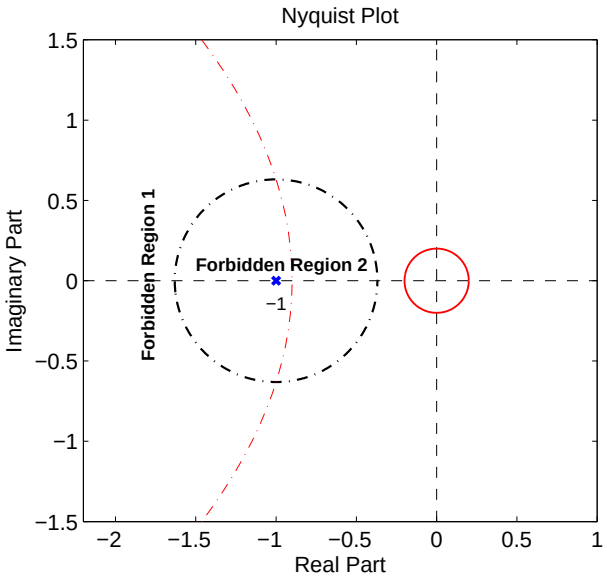

Figure 3.7: Frequency dependent forbidden regions in the Nyquist plane to ensure stability.

high frequency region to provide more robust stability for the large phase variations that are inherent in physical systems. This restriction can also be set via a circular region (solid) with the radius c and the origin at (0,0) in the Nyquist plot. We can state all the constraints in the nyquist plane together as follows

$$\begin{aligned} &\Re\{L(\mathbf{x},\omega)\} \geqslant -d_1\, \Im\{L(\mathbf{x},\omega)\}^2 - d_2, \qquad \forall\omega \in [0,\infty) \\ &|1 + L(\mathbf{x},\omega)| \geqslant b, \qquad \forall\omega \in [0,\infty) \\ &L(\mathbf{x},\omega) \leqslant c, \quad \forall\omega \in [\varpi,\infty), \end{aligned} \tag{3.30}$$

where the variables are real numbers with $d_1 > 0$, $d_2 > -1$ and b and c in the interval (0,1).

3.5.4 Phase and Gain Margin

In the preceding section we declared the stability margins in a mathematical proper manner. If we want to translate these set of prerequisites to more common and intuitive stability constraints (i.e. gain margin GM in dB and phase margin PM in degree) of a typical design task we can state the following two relations from

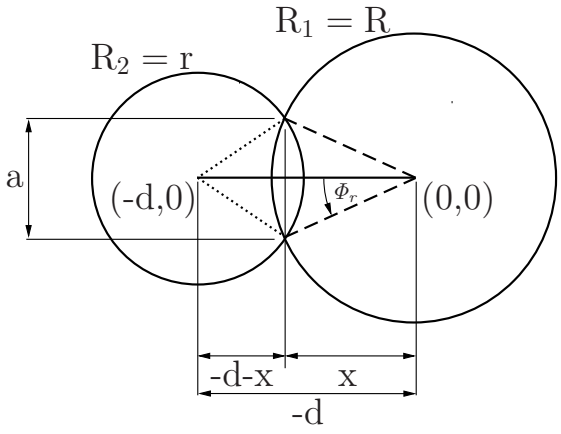

Figure 3.8: Intersection of two circles representing the unit circle and the "Forbidden Region 2". R equals one for the unit circle and r=b, where b represents the radius for the constraint against excessive noise amplification. The phase margin Φ_r (PM) denotes the positive angular distance from $-\pi$.

Fig. 3.8

$$\begin{aligned} \mathrm{GM} &= 20\log_{10}(1-b) \\ \mathrm{PM} &= \frac{180}{\pi}\arctan\left(\frac{a/2}{x}\right). \end{aligned} \tag{3.31}$$

The positive phase margin can be calculated with the geometrical properties of two intersecting circles. Further mathematical relations are found in Appendix A.

3.5.5 Pros and Cons

A big advantage of the nonlinear optimization approach is the intuitive formulation of the constraints in the complex plane, which allows us to provide necessary and sufficient stability. They can be translated into inequality constraint equations in Matlab to set up a constraining function for the optimization tool *fmincon*. The optimizer can be used with the active-set approach to find a minimum solution for the multidimensional objective function. The objective function (i.e. formula of minimizing the closed loop, Eq. (3.22)) with the constraints on the filter order form a non-convex problem, which might result in a local minimum. Therefore, the initial point is utmost important and we can not guarantee an overall best solution.

Chapter 4

Measurement

The next sections emphasize on measurement procedures to define the impact of different wearing situations on the frequency response of a secondary path. We can attest that there is a typical wearing situation per definition for headphones, which is intended by the manufacturer. In case of closed ear-cup headphones, the standard wearing situation would be if the headphones are put on symmetrically and circumaural (around-the-ear) with no pressure on any of the mechanical parts from outer forces. There are many wearing situations that occur during headphone use which change the magnitude or phase values of the secondary path, whether it is due to mechanical force or leakage.

4.1 Measurement - System Identification

To identify the electro-acoustic system from the loudspeaker to the microphone, an impulse response measurement can be used. The first investigations of the time signal showed that one can especially distinguish between the normal wearing situation and the pressed case (see Fig. 4.1, cf. Sec. 4.5). The time instants between these two wearing scenarios show that noise due to the deformation of the mechanical parts (i.e. deformation of the casing and ear pads) is introduced, which makes the investigation at this specific time instants not productive.

From this conclusion an exponential sine sweep is used for the impulse response measurements during situations where constant force (or no force - standard wearing situation) is applied onto the mechanical parts of the headphones. For reproducing

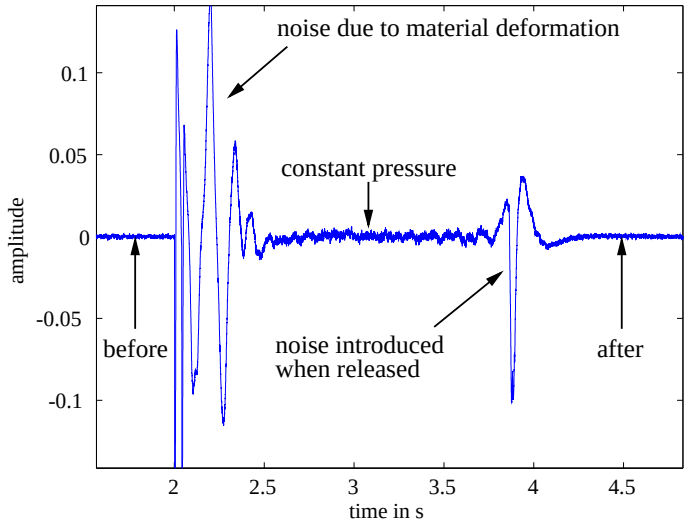

Figure 4.1: Measurement of headphones with pink noise as excitation signal. The time signal shows the normal wearing situation, when a force is applied on the mechanical parts, the time where the ear-cups are constantly pressed against the head, the noise which is introduced due to the release and then again the state of the standard fitting.

this measurement scenarios with different headphones a measurement fixture is presented in this chapter (see Fig. 4.5 in Sec. 4.3).

4.2 Measurement Setup

For measuring the secondary path the following setup is used:

- RME Hammerfall Dsp Multiface II
- AMS Evaluation Board AS3435 v1.2
- Measurement Notebook and Software
  - Puredata v0.34.4 extended
  - AMS Evaluation Board Software 1.1.13.0
- different headphones (David Clark, Samsung, Ultimate Ears).

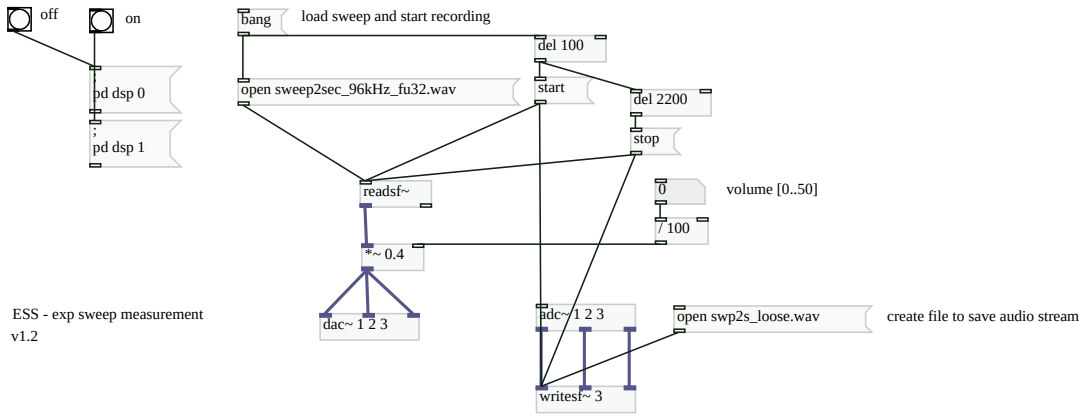

Figure 4.2: Puredata patch to play back the exponential sine sweep (ESS) and record the audio sent back from the evaluation board.

The Measurement notebook is equipped with the audio card, where a stereo signal is send to the AMS Evaluation Board. The evaluation board is only used for its audio amplifiers, where the input signal is fed to the loudspeakers and the picked up signal from the microphones is send back to the audio card. As a reference signal the audio output is hard-wired to an input of the sound card.

The software used for the play back is puredata, which provides a graphical interface to generate measurement signals, play back and record audio (see Fig. 4.2).

Fig. 4.3 shows a schematic of the primary setup for the evaluation of the different secondary path scenarios.

4.3 Measurement Fixture for Reproducibility

Further investigations are made on the measurement fixture shown in Fig. 4.4 to guarantee reproducibility of the measurements. The measurement fixture was designed during this master thesis. It provides two discs to place the headphone into the fixture and its dimensions correspond to dimensions of an artificial head. There are 2 weights with 2kg, 2 weights with 1kg and one weight with 0.6kg to simulate different combinations of forces on the headphones. The weights are put on a platform which can be moved up and down on a rail. The average weight of a human head is 4.1kg (men), 3.6kg (women) and they are used as a reference [Cle72]. The impulse response measurement has to be made for each ear-cup separately. It

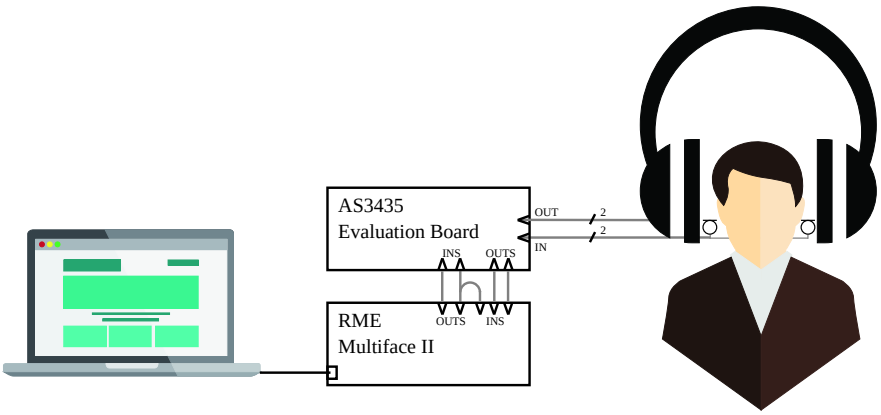

Figure 4.3: Schematic of the primary measurement setup for measuring the different secondary paths.

is possible to use a flat inlay or an ear simulator at the upper mounting position for the measurement, Fig. 4.5.

4.4 Position of the Error Microphone

The microphone to pick up the noise signal can be mounted at several positions inside the ear-cups. Different positioning can lead to distinguishable ANC performances. Still, it should be mentioned that the wavelength in the frequency band of interest is quite large in comparison to the distance of the mounting point of an error microphone to the loudspeaker. Common headphone manufacturers position the microphone in front of the loudspeaker and therefore also in front of the ear canal, which leads to minimal phase lag and the flattest phase response [GMK05]. A disadvantage can lie in this fixation point if the distance can be changed due to physical pressure on the ear-cups. That is why especially manufacturer for aviation headsets embed the microphone in a rigid plastic hemisphere in front of the loudspeaker (see Fig. 4.6 and 4.7). Another large influence on $S(s)$ has the fitting of the headphone on the user's head. The differences in the secondary path can not be neglected if a optimal filter that guarantees stability is demanded. This can be seen in the next section.

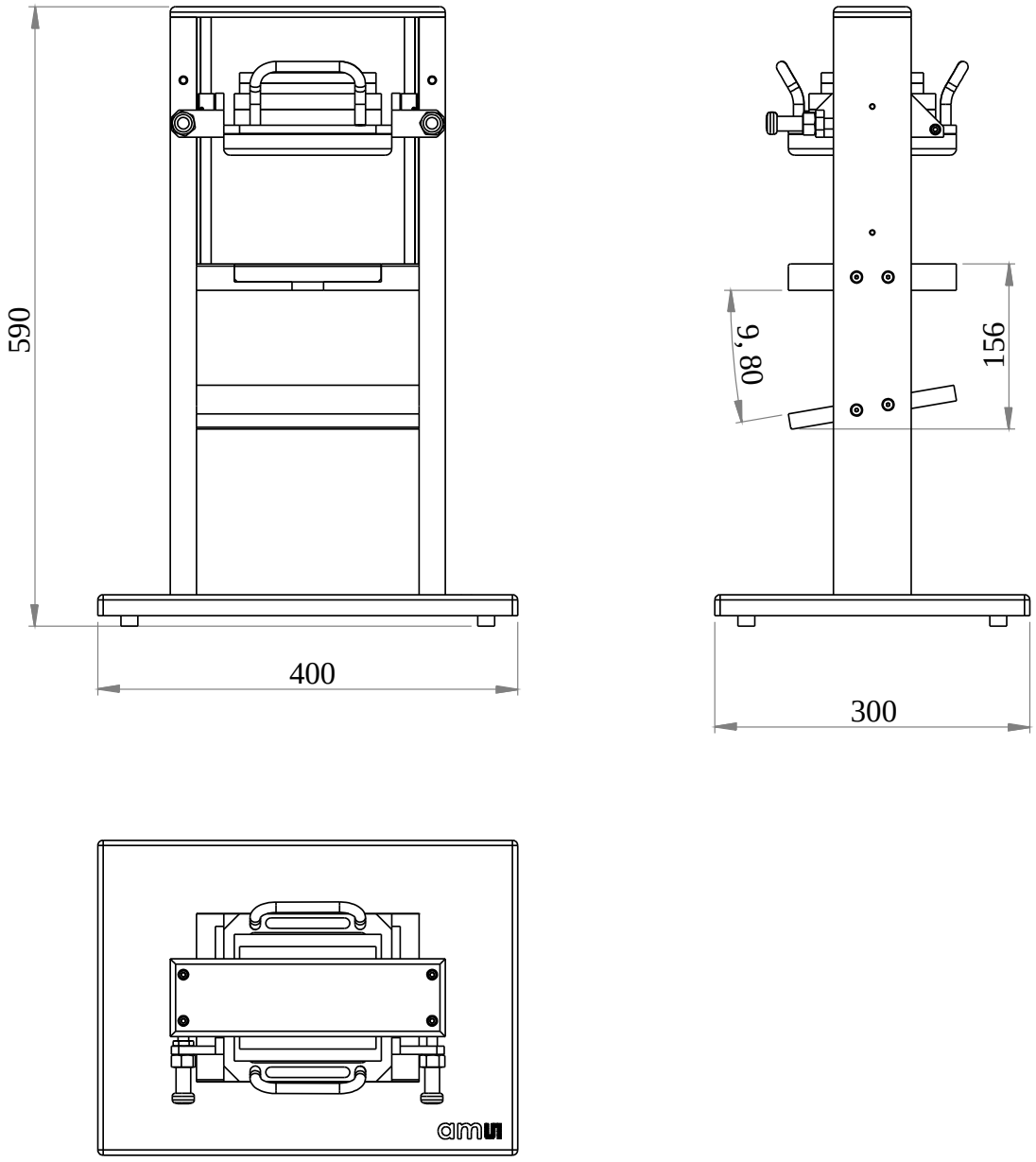

Figure 4.4: Schematic of the measurement fixture used for further evaluations. The fixture is build to guarantee reproducibility. It is possible to insert different discs at the upper mounting position (e.g. ear simulator, flat inlay).

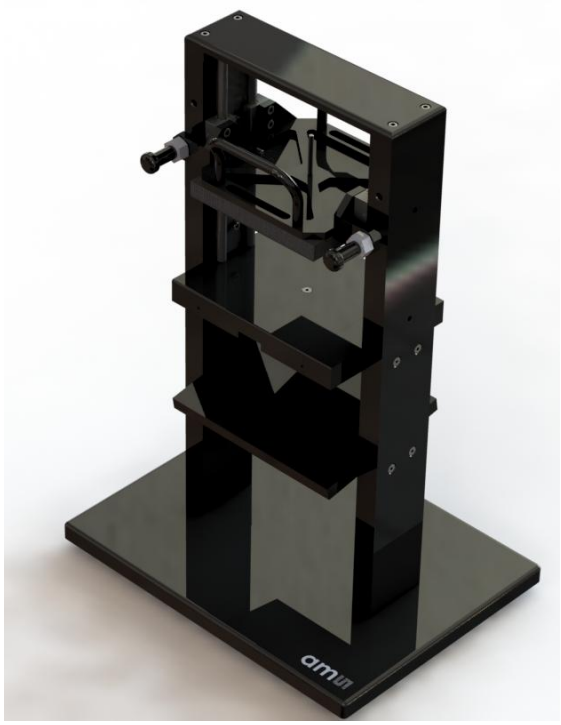

(a) without weights and flat inlay

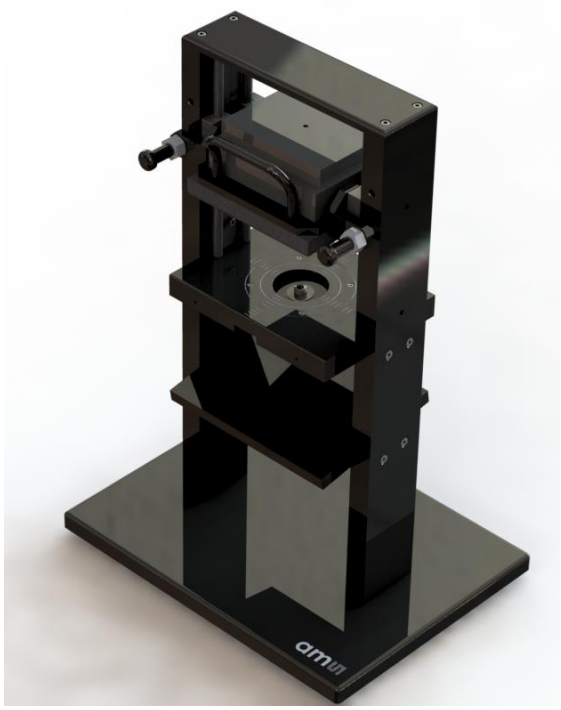

(b) with weights and ear simulator mount

Figure 4.5: Measurement fixture.

Figure 4.6: Headphones with microphone embeded in a rigid plastic hemisphere pointing away from the loudspeaker.

Figure 4.7: Headphones with different microphone positions. left: headphones with the microphone positioned next to the loudspeaker. right: aviation headset with the microphone positioned in a 90° angle to the loudspeaker.

4.5 Measurement Scenarios

Example of Misuse 1: If headphones are equipped with an ANC unit, typically a button (or anything similar) to switch the noise control on and off is integrated. Nevertheless, it does occur that the ANC is still on when the headphones are taken off. In that case the air can flow outside and this leads to very low magnitudes in the low frequency region. Also the phase values in regard to the normal wearing situation changes to a less steeper contour.
Example of Misuse 2: If the headphone user does lean onto a headrest (e.g. in a train cabin or airplane seat) the cups will be pressed against the ear/head which results in higher sound pressure inside the ear-cups due to reduction of the air volume and to a possible displacement of the error microphone if not fixed onto a rigid hemisphere.
Example of Misuse 3: If the ear-cups do not fit circumaural (e.g. headphone user wears glasses etc.), leakage is introduced. Leakage does also lead to a loss of sound pressure at the microphone inside the cups. Furthermore, unfavorable reflections at the temples of the glasses or at the pinna can occur and introduce more peaks and nulls in the frequency response as for the standard wearing situation which has a relatively flat frequency response (see Fig. 4.8, cf.[GMK05]). Following cases should be defined: **loose** - i.e the ear-cups are misplaced, **open** - i.e. the headphone is taken off and **pressed** - i.e. external force is put on the ear-cups or mechanical parts and **onhead** - i.e. the standard fitting (nominal secondary path). The first three types each could of course hold even more specific classifications on the positioning of the headphone. In Fig. 4.9 it is shown how the wearing situations result in different frequency responses.

If one wants to enhance the optimization process to variations in the secondary path it is advisable to include all misuse scenarios in the constraining function of the optimization task to provide stability under all circumstances. However, not every misuse scenario has the same impact on the phase and gain margins. It is sufficient to consider the worst case frequency responses which have the phase values closest to $-\pi(2n-1)$ for $n \in \mathbb{N}$ and those with the largest amplitude responses (worst-cases).

It is also possible to set up a worst-case synthesized frequency response (SYN)

Figure 4.8: Misplacement of the headphones on a dummy head. Leakage can occur if the fit is not like intended. Glasses can also introduce leakage and lead to unfavorable reflections at the temples of the glasses [GMK05].

to build a dense set of constraints for the optimization procedure. This is achieved if we take the envelope of the highest magnitude and the phase values closest to -$\pi(2n-1)$ of all measurement scenarios.
This can provide computational efficiency, because the size of the constraining vector shrinks at least by the factor 0.5. Note: this synthesized frequency response does not represent a real physical secondary path.
From Fig. 4.9 it can already be seen that the secondary path of the pressed headphones has the largest amplitude response and represents the worst-case for almost the whole bandwidth, but still does not hold the worst-case phase response.

As mentioned before, we can further fan out the definition of the different measurement positions. The pressed case can be also investigated for different scenarios like a slight offset of the headphones towards the front or back. Both misplacements result in similar frequency responses. Although it is to mention that parts of the frequency responses show worse behavior for the phase values than the pressed case with no offset and need to be considered, strictly speaking.

Another interesting fact for manufacturers is the case where the stability of an ANC headphone is tested with a human hand. If a hand is put in front of the loudspeaker and microphone inside the ear cup, we recognize significant lower

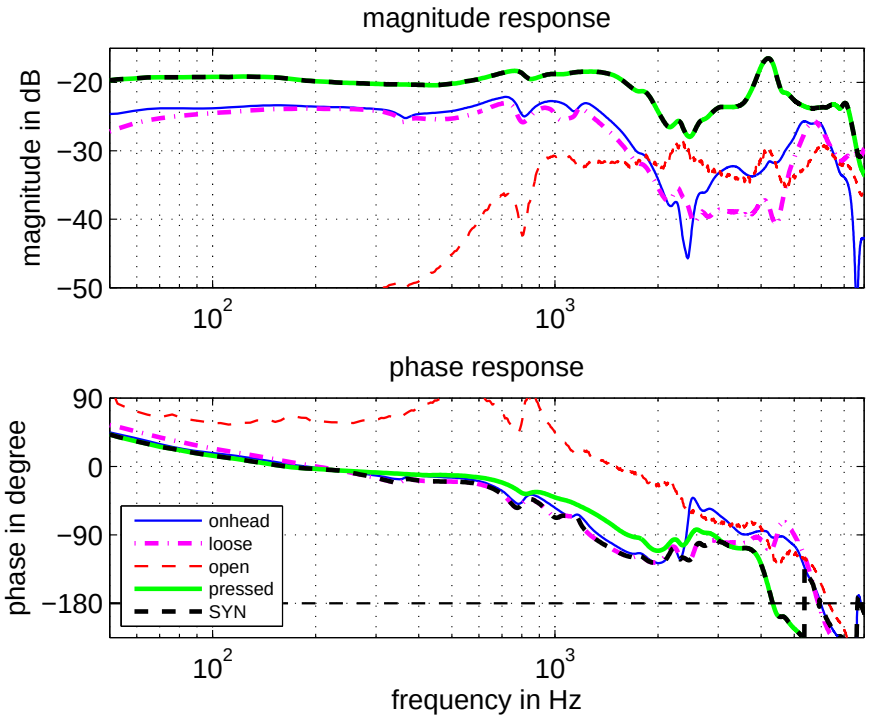

Figure 4.9: Measurement scenarios: The case when the headphone is pressed against the ear yields a frequency response with the largest magnitude and a fast falling phase. The opposite result is seen when the headphone is not put on (open). It is not possible to use only one measurement to define an overall worst-case, although we can construct a synthesized frequency response out of the worst-case pieces of all measurements (SYN).

magnitudes in the low frequency region (below 500Hz) and higher magnitudes in the region above than for a nominal secondary path (onhead). This is of course due to the fact that sound waves with longer wavelengths travel around the obstacle and shorter do not. The frequency response could be seen as a combination of the leakage and pressed case, cf. Fig. 4.10. The phase response around 2kHz shows similar values like for the nominal secondary path, but the magnitude values are at least 10dB higher. This leads to instability if a filter is designed for the standard fitting case and this test is carried out. Still, it is necessary to mention that such a procedure does not represent any real-life wearing situation.

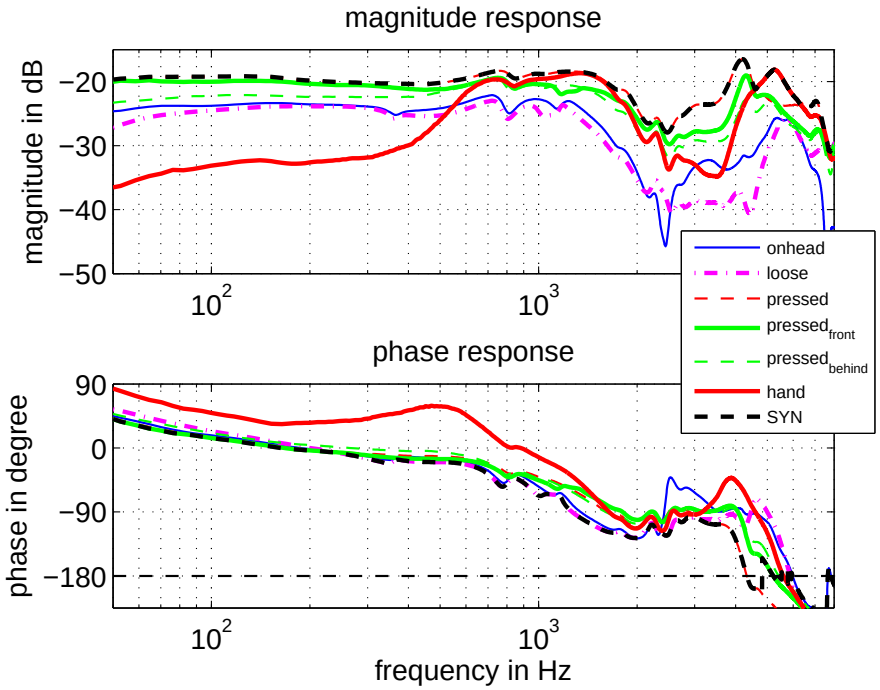

Figure 4.10: Measurement scenarios: The case when the headphone is pressed against the ear is now further investigated for different misplacement scenarios. Especially different phase values can be exhibited. A typical manufacturers test - a hand is put in front of the loudspeaker and microphone - results in a frequency response which could be interpreted as the combination of the leakage and pressed case. This scenarios together lead to a new worst-case synthesized frequency response.

Chapter 5

Performance Evaluation

The next sections present the performance evaluation of the approaches presented in chapter 3. First, investigations on different parameters for the optimal filter design in the cepstral domain (linear optimization problem) are presented. After that, an evaluation of the nonlinear design approach is made. Each approach has its advantages and disadvantages in terms of usability and convergence. At last, an investigation on the performance of the optimization process for a constraining function consisting of a set of worst-case secondary paths is treated.

5.1 Evaluation of the Optimal Filter Design in the Cepstral Domain

For designing an optimal filter in the cepstral domain, the design constraints and their impact on the ANC performance need to be considered. We have defined a passing section, a "don't care region" where the open-loop magnitude can roll-off and a stop section. The upper frequency bound of the passing section is f_{pass} and the lower frequency bound for the stop section f_{stop}. The performance for different combinations of f_{pass} and f_{stop} are investigated. Furthermore, the impact of changing other design constraints as the restrictions on the filter gain or open-loop gain in the stop section is evaluated.

5.1.1 Open-Loop Roll-Off Behavior and Don't Care Region

Since the open-loop gain is forced to roll-off after the frequency f_{pass}, the results show that the maximum noise rejection is achieved a little bit below this frequency bound, seen in Fig. 5.1(a)(b). For the "pass-frequency" $f_{pass} = 700$Hz this is not true, although the roll-off behavior shows at least similarities to the designs for $f_{pass} = 300$Hz and $f_{pass} = 500$Hz, seen in Fig. 5.2(a)(b). It can be shown that the broader the region to achieve noise rejection, the lower is the overall noise reduction. This is due to the waterbed effect mentioned in Sec. 2.2.3, where we denoted that the sum of the areas below and above the sensitivity function over all frequency bins has to be 0dB for a stable closed-loop system. This means there is a trade-off between a good noise rejection and the bandwidth.

A design criterion besides the constraint f_{pass} is how broad the "don't care region" is chosen. To evaluate the behavior, the "stop-frequency" (i.e. the lower bound of the stop section) is chosen $\frac{5}{4}$, $\frac{5}{3}$ and 3 times the "pass-frequency". The results in Fig. 5.1(a)(b) show that a broader "don't care region" yields in a better performance. For $f_{pass} = 500$Hz the improvement is still inherent, but not that significant because of the waterbed effect, which leads to a broader noise amplification area for high frequencies around 1,2 and 3kHz as depicted in Fig. 5.1(c)(d). The decision on how broad the passing section is chosen, results again in a trade-off between the maximum magnitude for noise rejection and the broadness of the frequency range where noise rejection needs to be achieved. Typically the maximum magnitude is chosen over the broadness, because the effect is more significant to non-expert listeners (i.e. average consumer of ANC headphones). Still, from a psycho-acoustical view point a broader frequency range could be more efficient, but this topic will not be investigated within this thesis.
Furthermore, it should be stated that if the "don't care" region is more narrow, the open-loop behavior has to have a steeper contour in the "don't care" region and this consequently has to result in a higher filter order.

5.1.2 Filter and Open-Loop Gain in the Stop Section

Another design constraint to consider is the gain restriction on the optimal filter. The notation of the linear constraints in the cepstral domain allows more than

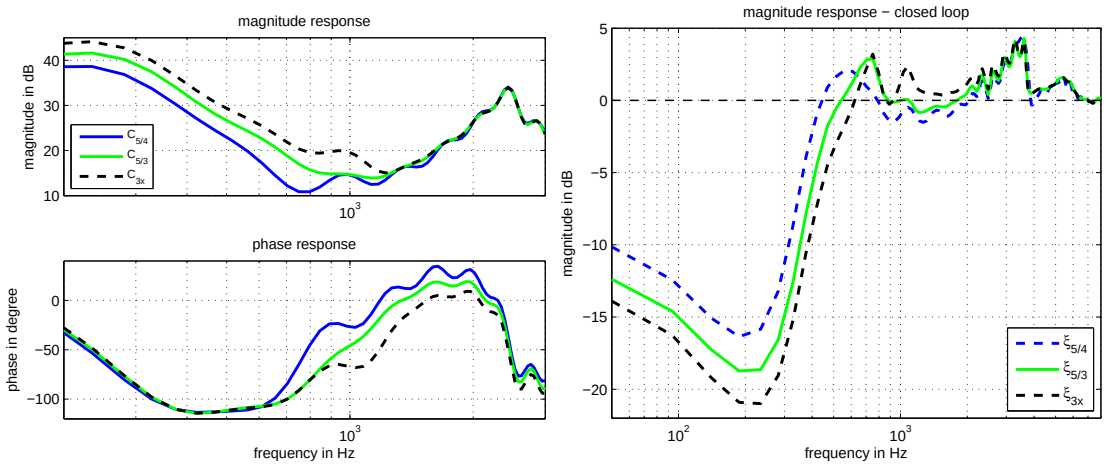

(a) $f_{pass} = 300Hz$ (b) $f_{pass} = 300Hz$

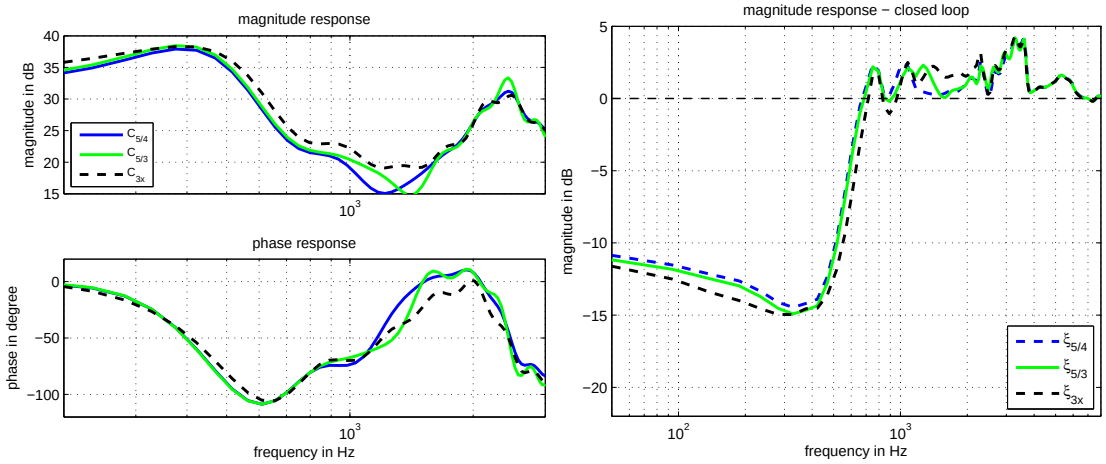

(c) $f_{pass} = 500Hz$ (d) $f_{pass} = 500Hz$

Figure 5.1: Evaluation of the optimal filter for different design specifications. a) and b) depict the filter design and sensitivity functions for differently broad "don't care regions". The best result is achieved if f_{stop} is chosen 3 times higher than f_{pass}. c) and d) show that the broader the passing section is, the lower is the maximal achieved noise reduction value.

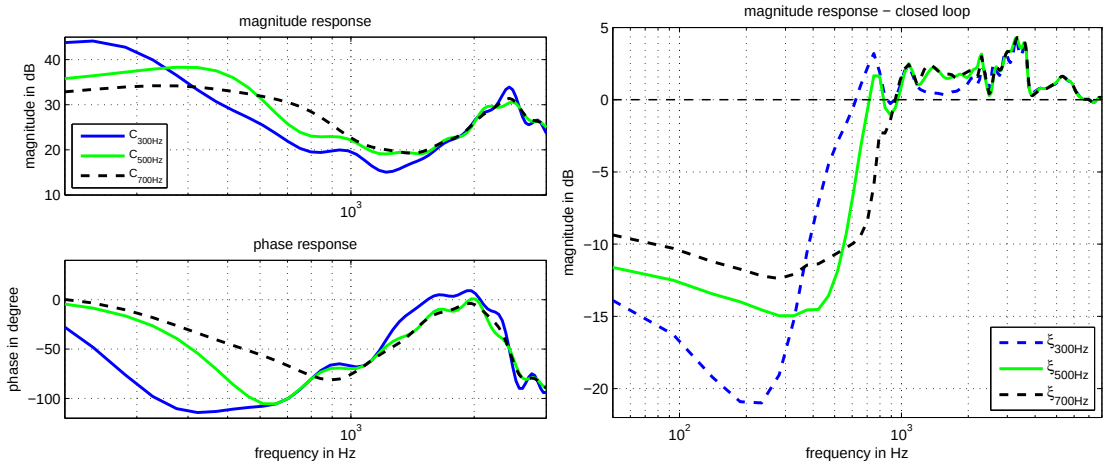

(a) (b)

Figure 5.2: Evaluation of the optimal filter for different design specifications. a) and b) depict the comparison of the three design approaches.

only to specify the three regions (pass, stop and "don't care") to control the open loop. It is also possible to restrain the filter gain. Large filter magnitudes for high frequencies in the stop section are unwanted because of internal circuit noise amplification and increased power consumption. This can be prevented if the filter is designed to stay below a certain level. Fig 5.3 shows filters where an amplification higher than 10dB for a frequency above 1.5 kHz is forbidden. This restriction leads to a more conservative sensitivity function with 6dB less noise rejection at frequencies of pronounced ANC, which can be seen in Fig. 5.4b.

Closely related to the noise rejection is the noise amplification. As mentioned in the previous chapters, it is crucial to limit the maximal noise amplification around 4dB. The constraint for the open-loop gain in the stop section restricts the maximal noise amplification and can be denoted for the worst-case scenario (i.e the phase values -π) as

$$20\log\left|\frac{1}{1+\alpha e^{-j\pi}}\right| = 20\log\left|\frac{1}{1-\alpha}\right|. \tag{5.1}$$

For most design cases, an open-loop gain of -10dB is chosen, which yields in a maximum noise amplification of $\approx$ 3dB. The design criterion for the open-loop gain in the stop section in the results shown in Fig. 5.1, 5.2, 5.3 and 5.4 is -8dB ($\widehat{=}$ max. noise amplification of 4.4dB), which has to be fulfilled in the frequency range from

f_{stop} to $f_s/2$.

The constraints on the phase values in the pass section demands stability and also restrains the filter design. If the open-loop magnitude has to stay below a certain dB value (achieved by the open-loop gain constraint in the stop section) the magnitude of the filter underlies a restriction, likewise. Typical values for the phase margin in the pass section would be around 55°. If the phase margin is chosen less conservative an uncontrolled overshoot of the sensitivity function in the frequency region around the transition from the pass section to the "don't care" region can occur.

5.1.3 Approximation of the Optimal Solution

The optimal filter shapes presented in this section show a fluctuating frequency response due to the behavior of the algorithm, which does not have restrictions on the length and the phase of the filter, apart from being minimum phase. We seek an analog filter design and the best way to do so is as an IIR filter representation. We can use an approximation algorithm like the one proposed by Steiglitz and McBride [SM65] and whose result is shown in Fig. 5.4. The resulting magnitude and phase contours fit exactly between the fluctuating frequency responses[1]. The filter with the gain restriction (of 10dB) starting at 1.5kHz can be approximated with a second order peak filter and the filter with the gain restriction starting at 4kHz can be easily approximated with an 4th order filter ($\widehat{=}$ combination of two peak filters). If the filters are approximated, again an investigation in terms of stability has to be made. Therefore, a look at the Nyquist plot and the impulse response of the closed loop gives the necessary information if the approximated filter still yields a feasible solution.

[1] However, this can not be guaranteed.

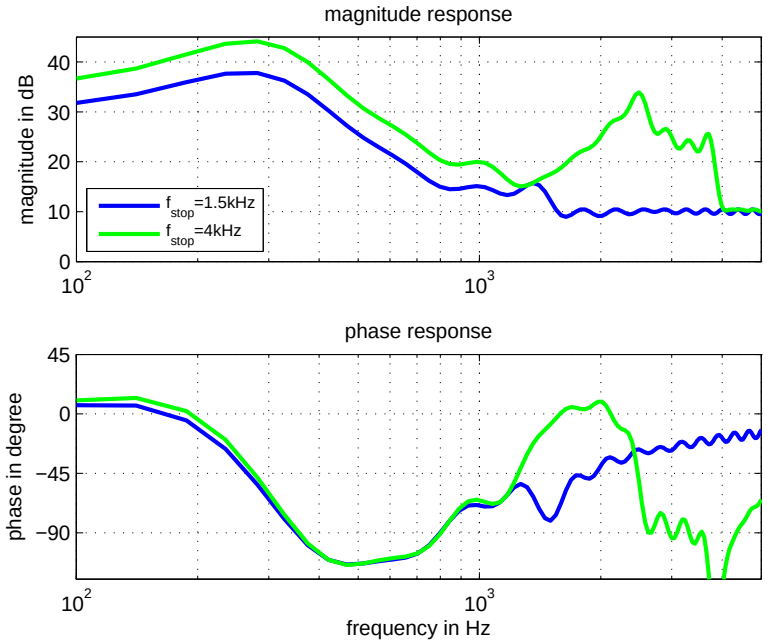

Figure 5.3: Comparison of two optimal filters for a nominal secondary path for different filter restrictions. The first is not allowed to exceed 10dB starting at 1.5kHz and the second one up from 4kHz.

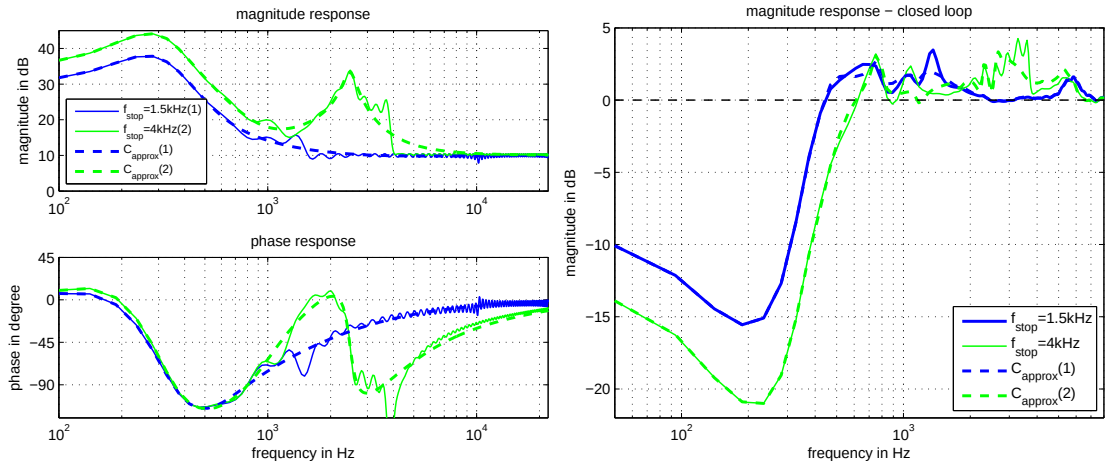

(a) (b)

Figure 5.4: Comparison of the interpolation and performance of the two optimal filters for a nominal secondary path for different filter restrictions. The Approximation is made via the Steiglitz-McBride algorithm for the order=2 (dashed blue line) and order=4 (dashed green line) with 10 iterations.

5.1.4 Comparison to a Manually Designed Filter

In Fig. 5.5a we see the manual filter design for the same headphones. A classic approach is to design a filter out of the combination of a peak and notch filter to achieve a noise rejection with the gain of the peak filter. The notch filter is used to raise the phase contour for higher frequencies and needs to fulfill a phase margin of 60°, which is a common reference value in the manual design. The resulting sensitivity function is shown in Fig. 5.5b. The comparison shows that the approximated solution of the optimizer yield noise reduction for a broader frequency range and still has a lower noise amplification than the peak/notch combination. It can be seen that already a 2nd order filter can result in an at least similar ANC performance.

It shall be denoted that this comparison includes a frequency range of 20Hz to 32kHz by a sampling rate of 96kHz. Nevertheless, the phase response of the various measurements for lower frequencies than 20Hz show a clear tendency towards the phase value $+\pi$. Therefore, another constraint to prevent instability at very low frequencies is crucial for the proposed method. This can be achieved by a "stop" section at a starting frequency of 10Hz, which is a typical lower frequency bound for high quality ANC headphones. Here, the design task is to provide that the open-loop gain stays below unity in the region where the phase value lies above $+\pi$.

5.1.5 Summary

This section showed that the optimal filter design can be described quite intuitive with some common margins for the open loop and for the filter to yield a stable solution. The optimizer is therefore quite handy for ANC filter design engineers. The resulting frequency response can be used as a design template for the manual filter design or it can be approximated with the Steiglitz-McBride algorithm as it was shown in this section. Nevertheless, it is crucial to do a repeated investigation of the stability with the approximated filters. The linear optimization task can be made for an arbitrary frequency resolution. It is sufficient to use a higher resolution in the low frequency domain and lower resolution in the high frequency region. This is a typical advise for filter design on digital computers. In regard of

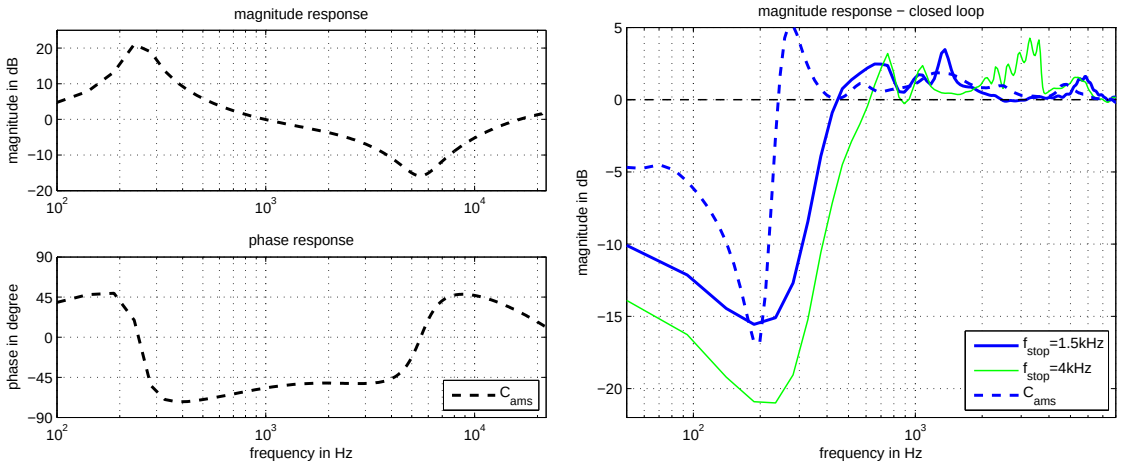

(a) (b)

Figure 5.5: a) Manually shaped filter for a nominal secondary path. b) Sensitivity function. The phase margin of 60° has to be fulfilled for the frequencies where the open-loop gain is above unity.

the number of cepstral coefficients used for the optimization procedure it can be stated that more than 256 coefficients do not bring any improvement. On the other hand it can be stated that at least 128 coefficients should be used to get a proper representation with no loss of information. Low quefrencies (i.e. "frequency" bins in the cepstral domain, cf. Sec. 3.4) represent the energy of a frequency domain signal, whereas higher quefrencies represent the harmonics of a frequency domain signal. Furthermore, it should be denoted that the passing section is weighted with the weighting functions of the hearing model from Sec. 3.1 to emphasize the optimization process more onto the frequency region where the human auditory system is more sensitive.

5.2 Nonlinear and Non-Convex Optimization for a Limited Filter Order

The first approach in the cepstral domain stated the constraints in a linear relation. The second approach used within this thesis uses nonlinear constraints on the open loop which are stated in the complex plane[2]. Another restriction is made on the numerator and denominator of the filter, which results in a non-convex optimization. This is one disadvantage, because the optimization might end in a local minimum. Nevertheless, the results show acceptable solutions if the starting point is well chosen.

5.2.1 Performance Evalution of a 2nd Order Filter Design

The evaluation is targeted to yield a comparison between the two presented algorithms. However, a necessary fact for the comparison is that the linear optimizer is minimizing the objective function in an H_∞-sense (max. amplitude) and the nonlinear optimizer in a H_2-sense (max. energy). Furthermore, the nonlinear approach might result in a local minimum which is dependent on the initial point. The next plots will show the results of 2nd order filters with almost the same boundaries on the optimization process as in the approach in the cepstral domain.

The constraints chosen for the evaluation are 4.4dB as the maximum allowed noise amplification, a maximum of 10dB filter gain above 4kHz and the order of the control filter is restricted to 2. In comparison to the evaluation in Sec. 5.1 a weighting is applied to the sensitivity function (which is already weighted with the weighting functions of the hearing model from Sec. 3.1). This weighting is denoted as a rectangular window $W(\omega)$ with 0dB up to the "pass-frequency" (300Hz, 500Hz and 700Hz) and $-\infty$ dB elsewhere. Of course the term "pass-frequency" is misused for the purpose of comparison because the nonlinear approach has no pass, "don't care" and stop region. The open-loop gain is restricted to stay below -10dB for 3 times the "pass-frequencies": 300Hz and 500Hz[3].
Fig. 5.6 shows the three different optimal filters for the above denoted constraints.

[2]To be more precise: in the Nyquist plane.

[3]The open-loop gain restriction for 700Hz is set to 1.5kHz. Higher stop frequencies for the 700Hz "pass-frequency" did not yield a feasible result in the linear optimization approach.

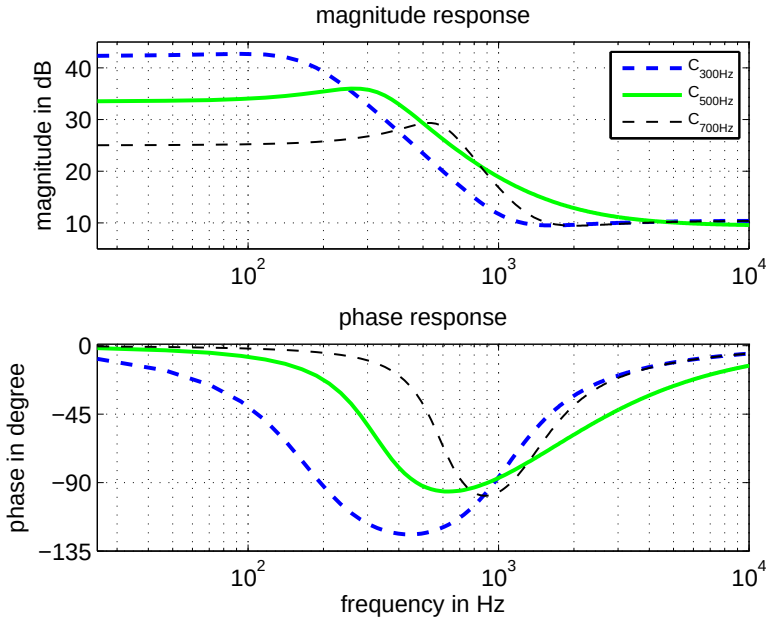

Figure 5.6: Results for the optimal filters of the nonlinear approach. The initial point is set as a 2nd order chebychev filter with a cut off frequency about 100Hz below the "pass-frequency" (i.e 300Hz, 500Hz and 700Hz).

The proposed filters are 2nd order filters, which can be clearly seen from their phase responses. The sensitivity functions of these filters show that the weigthing and the initial points lead to different solutions compared to the approach in the cepstral domain, which is due to the non-convex property of the optimization problem, seen in Fig. 5.7.

If the initial filter is set with coefficients of a peak filter and the maximum filter gain for low frequencies is constrained to stay below 10dB the results in Fig. 5.8 and Fig. 5.9 can be achieved. The optimizer does not propose a peak filter with a typical pole and zero combination close to the imaginary axis. Instead of two conjugate complex zeros, one zero is located on the real axis close to the origin of the coordinate system and one zero is located farther away in the left half plane (see Fig. 5.10). This introduces an unequal compensation of the gain before and after the center frequency of the peak in the magnitude response.

The plots of the sensitivity functions reveal that the best ANC performance can be denoted as the peak filter design with the "pass-frequency" set to 500Hz. The

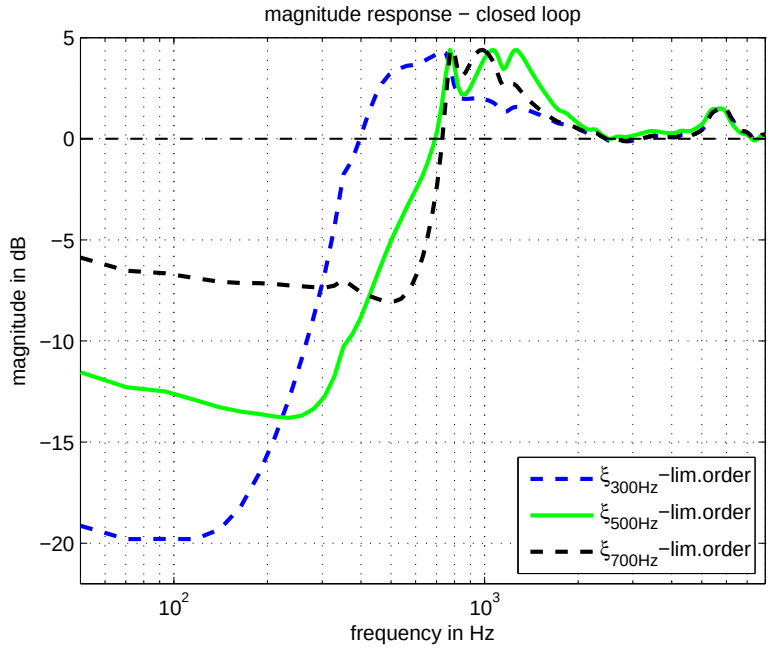

Figure 5.7: Sensitivity functions for a nominal secondary path and the optimal filters calculated with the three different initial points and weighting functions.

sensitivity function of this design shows better performance than the one achieved with $f_{pass} = 300$Hz and $f_{pass} = 700$Hz, except for a higher noise amplification in comparison when $f_{pass} = 300$Hz.

The advantage of this design approach is the controllability via the Nyquist plot. We can plot the open-loop root loci for the different filter designs and have a visual control if the design constraints are met. The open-loops in the Nyquist plane resulting from the shelving-like control filters and the nominal secondary path are depicted in Fig. 5.11.

The comparison of the performance of the linear and nonlinear optimization approach for a bandwidth of 300Hz is shown in Fig. 5.12. The comparison shows the optimization approaches with a gain restriction of 10 dB starting at 1.5kHz. The optimal filter of the linear optimization, the filter approximation of the linear optimization as an IIR filter via Steiglitz-Mcbride and the IIR filter from the nonlinear optimizer are compared. The performance results depicted in Fig. 5.12b of the linear optimization (also the approximation) outrun the results of the nonlinear optimizer slightly in terms of noise amplification. However, it can be shown that

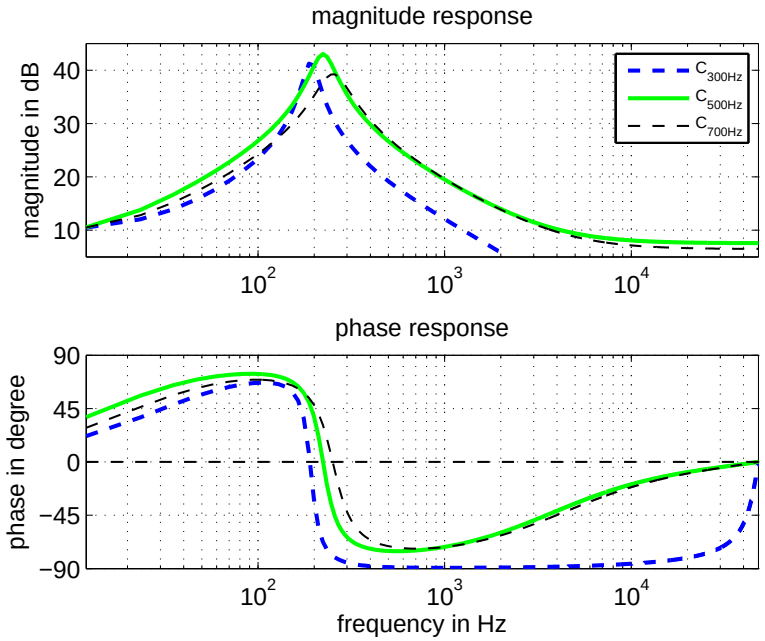

Figure 5.8: Results for the optimal filters of the nonlinear approach. The filter is initialized with a 2nd order peak filter. A gain restriction of 10dB is set for low frequencies.

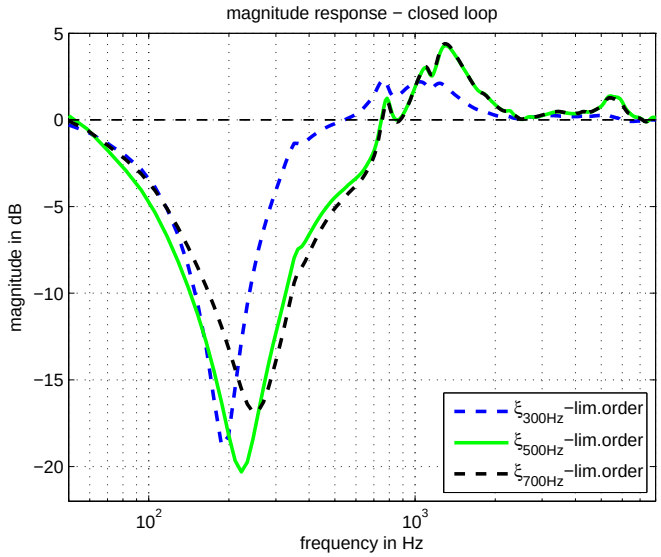

Figure 5.9: Sensitivity functions for a nominal secondary path and the optimal filters calculated with the coefficients of a 2nd order peak filter as initial point and a restriction on the filter gain for low frequencies of 10dB.

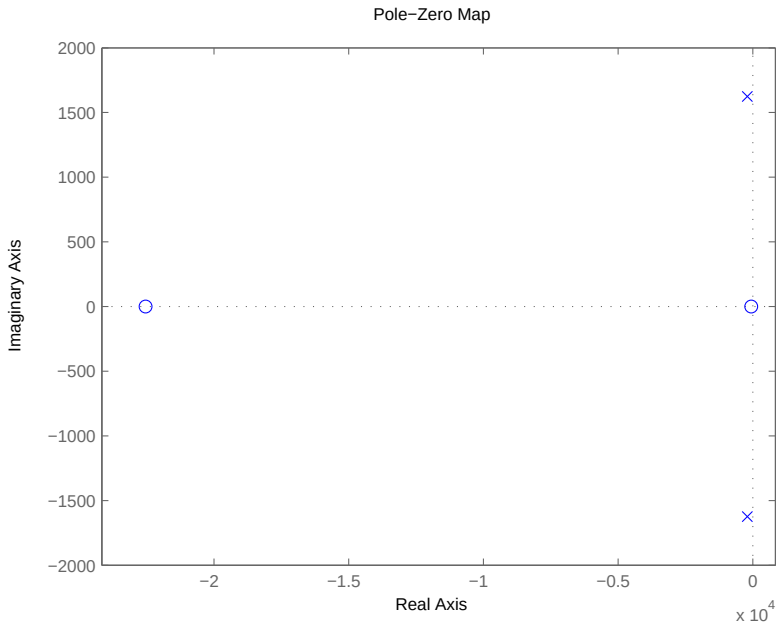

Figure 5.10: Pole/zero Map for the 2nd order peak filter for a bandwidth of 500Hz. The locations of the zeros lead to an unequal gain before and after the center frequency of the peak in the magnitude response.

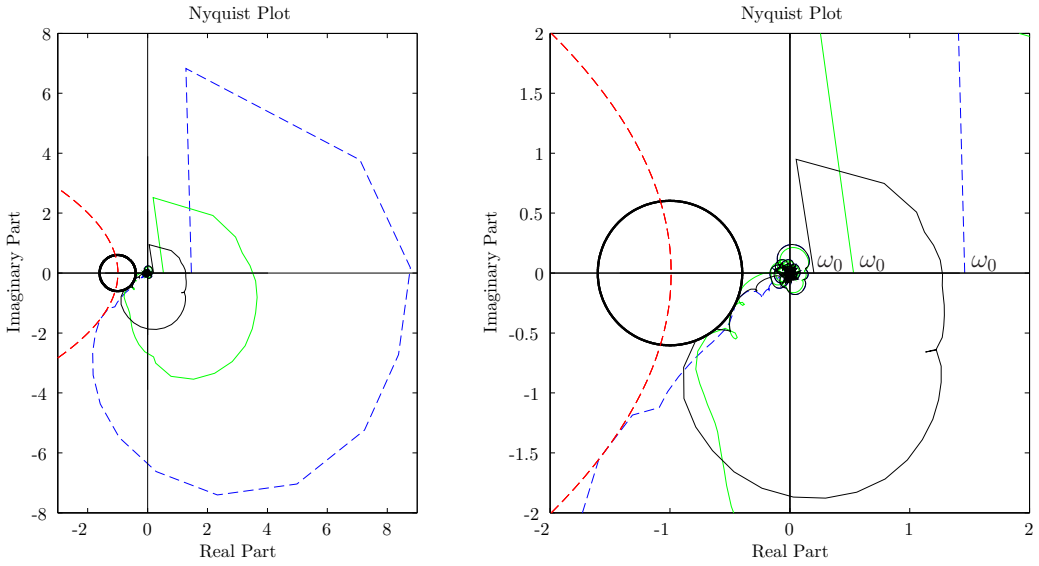

(a) (b)

Figure 5.11: a) Root loci of open-loops for the first design constraints. b) Zoom on the root loci starting and end points (i.e $\omega_0 = 0$ to $\omega = 2\pi\frac{fs}{2}$ at the origin).

the nonlinear filter achieves a better noise rejection in the frequency region around 200Hz.

5.2.2 Summary

The presented approach in this section has several advantages, especially in terms of constraining the optimization process with intuitive boundaries known from classic control theory. The direct and intuitive controllability of the constraints is another positive effect. The objective function is minimized in a H_2-sense, which emphasizes on the energy in the sensitivity function and not only on the maximum value like in the H_∞ optimization. However, the objective function is not convex and therefore it can not guarantee the best solution for the filter design. The initial point has a crucial impact on the optimization results. It is therefore not sufficient to use only one run-through. The optimization process needs to be repeated several times with different guessed initial points.

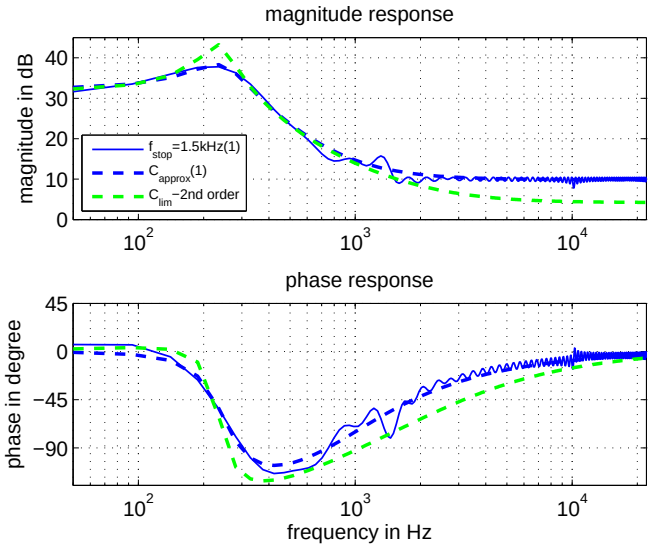

(a)

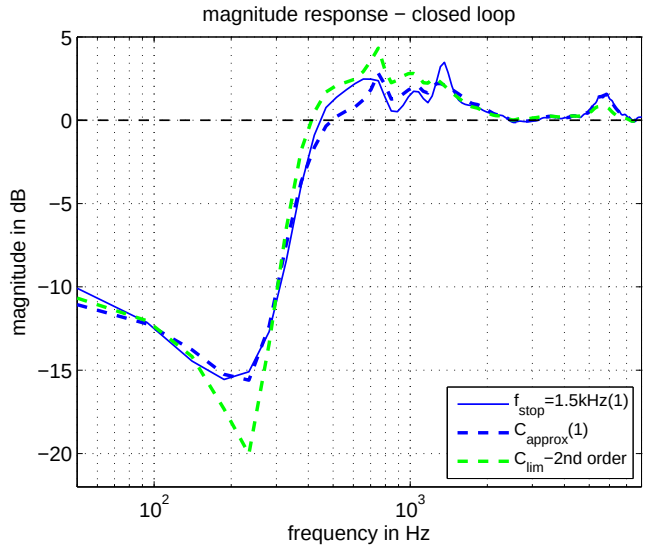

(b)

Figure 5.12: Comparison of the two optimization approaches for a bandwidth of 300Hz and with a gain restriction of 10 dB starting at 1.5kHz. In a) the solution of the linear optimization, the approximation of the linear optimization as an IIR filter and the IIR filter from the nonlinear optimizer are shown. In b) the sensitivity functions as a result of the filters used for a nominal secondary path from a) are compared. The results of the linear optimization (also the approximation) outrun the results of the nonlinear optimizer slightly in terms of noise amplification. However, it can be shown that the nonlinear filter achieves a lower overall magnitude for the frequency region of noise rejection at around 200Hz.

5.3 Filter Optimization with Worst Case Constraints

If we want to minimze the sensitivity function in a specific frequency region for more than one secondary path we can denote an objective function J that depends on a nominal secondary path S_n

$$\begin{aligned} &\min\ J(S_n(s)), \\ &\text{with subject to the constraining function: } f(\mathcal{S}) < 0, \end{aligned} \tag{5.2}$$

whereas S_n represents the secondary path of the intended wearing scenario and $\mathcal{S}$ holds all possible secondary path variations (i.e. plant uncertainty) to constrain the optimization process.

The variations in the secondary path depend on the fitting of the headphones (cf. chapter 4). Fig. 5.13 shows measurements of a normal wearing position (onhead), a scenario where the headphone is slightly off the normal position (loose), the case before the headphone is put on (open) and the case where the headphone is pressed against the ears. Due to the increased magnitude of the pressed secondary path, the gain of the control filter is necessarily smaller than it would be for the nominal secondary path. This can be observed in Fig. 5.14 which depicts the outcome of the optimization for different secondary path measures in the constraining function. It can also be seen that the synthesized secondary path leads to a more conservative control filter in comparison to the more processing intense optimization task which uses all physical worst-case secondary paths.

The performance of ANC for a set of secondary paths $\mathcal{S}$ can easily be assessed via the sensitivity function. For the first performance analysis we use the nominal secondary path together with the optimal filters $C_i(s)$ presented in Fig. 5.14 yielding

$$\xi_i(s) = \frac{1}{1 + S_n(s)C_i(s)}. \tag{5.3}$$

Fig. 5.15 shows that the filter which is designed for the nominal plant yields more noise reduction between 40Hz and 1kHz, but also gets closest to our maximum amplification constraint for the sensitivity function, which is $20 \log \max |\xi(s)| \leqslant 4\text{dB}$. As already mentioned in Sec. 2.2.3, we observe an amplification of higher frequencies

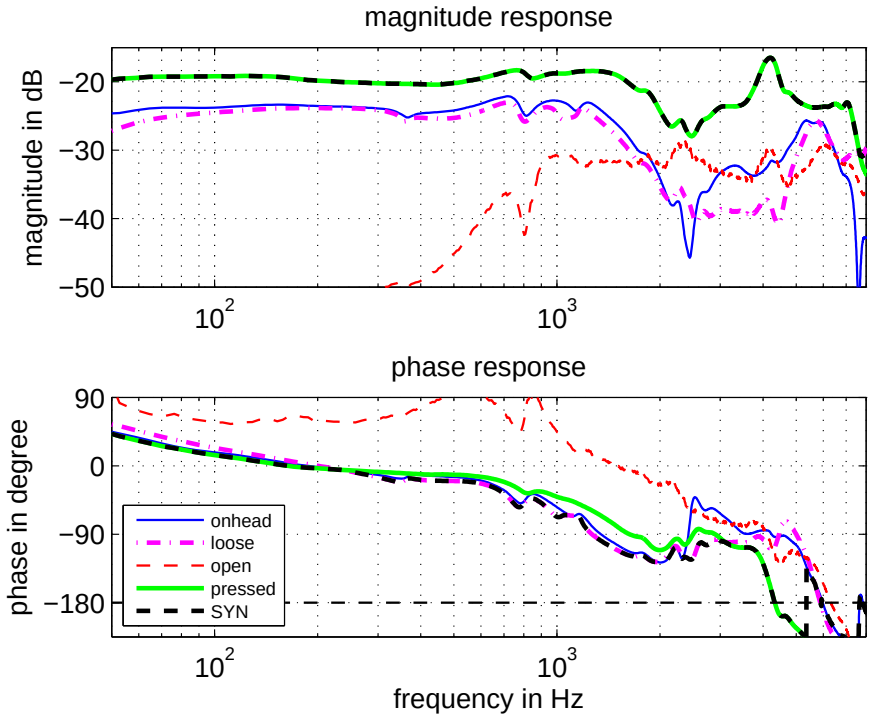

Figure 5.13: Measurement scenarios: The case where the headphone is pressed against the ear yields a frequency response with the largest magnitude and a fast falling phase. The opposite result is seen when the headphone is not put on (open). It is not possible to use only one measurement to define an overall worst-case, although we can construct a synthesized frequency response out of the worst-case pieces of all measurements (SYN).

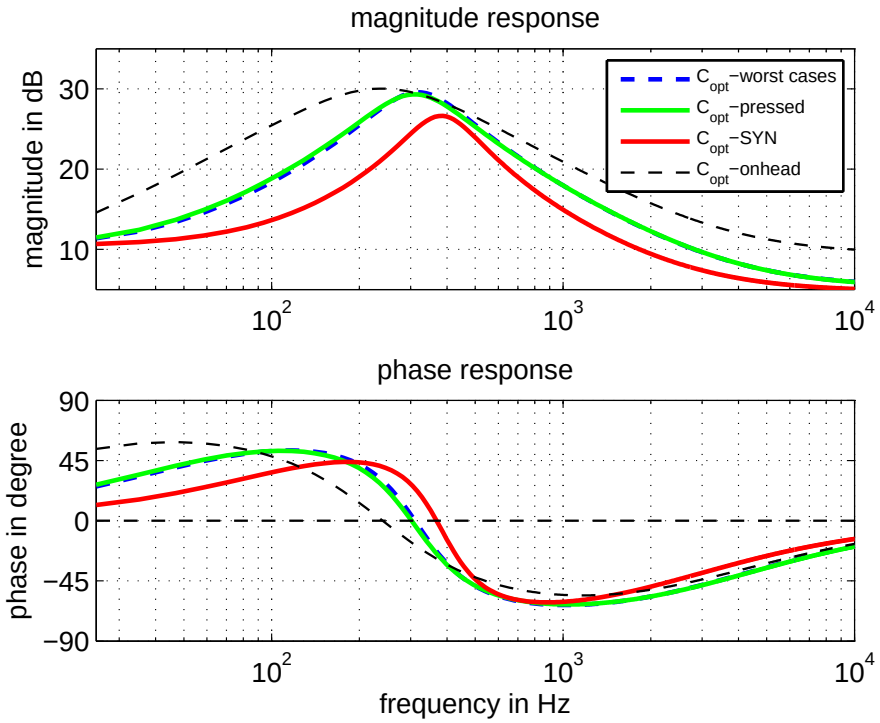

Figure 5.14: Outcome of the optimization for 2nd order optimal filters with different secondary paths in the constraining function: (i) all the measured worst case scenarios are considered, (ii) only the pressed secondary path is considered, (iii) a single frequency response which is piecewise synthesized from all measured worst cases is considered, (iv) only the onhead secondary path is considered. Synthesized constraints result in the most conservative optimal filter, whereas an optimization on the nominal secondary path leads to the opposite.

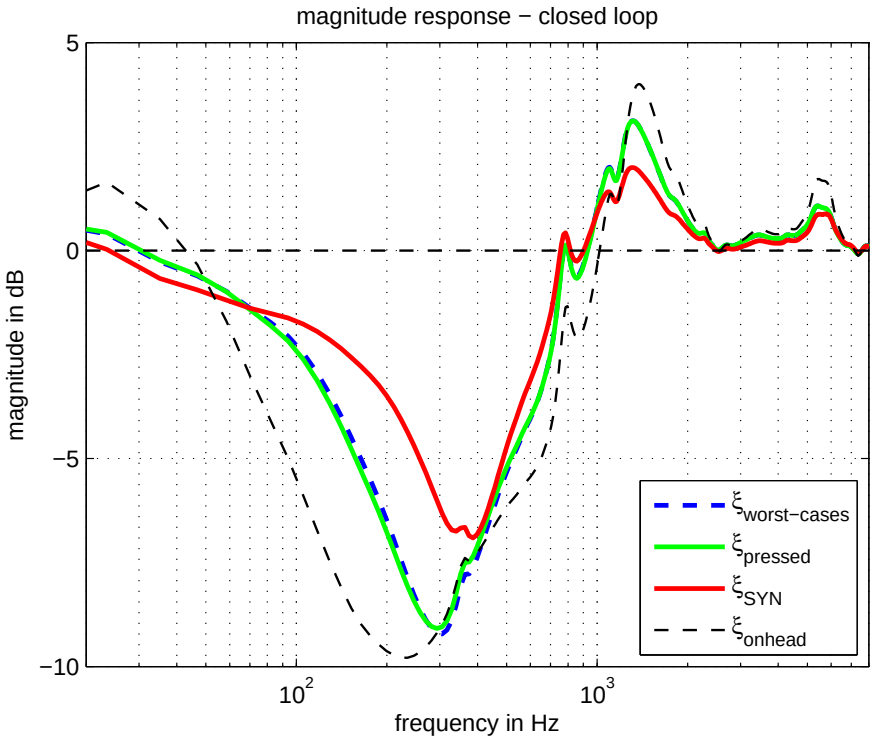

Figure 5.15: Performance analysis of 2nd order optimal filters in Fig. 5.14 applied to the nominal secondary path (i.e standard fitting of the headphone). The design constraint for the maximum amplification restricts the magnitude to be smaller or at least equal to 4dB.

in the trade-off to a good noise rejection in the lower frequency region.
In the second performance analysis, we use the pressed secondary path S_{press} to investigate the sensitivity function

$$\xi_i(s) = \frac{1}{1 + S_{\text{press}}(s)C_i(s)}. \tag{5.4}$$

In this case, the optimal filter designed for the nominal secondary path C_{onhead} violates the magnitude design constraint of $\xi(s)$ and causes a noise amplification of more than 7dB as can be seen in Fig. 5.16. All other filters meet the constraints, whereas the most conservative filter C_{SYN} achieves the lowest performance. Since S_{press} represents the worst case secondary path for almost the whole frequency range, the results of ξ_{press} and ξ_{wc} (including all worst-cases) are very similar.

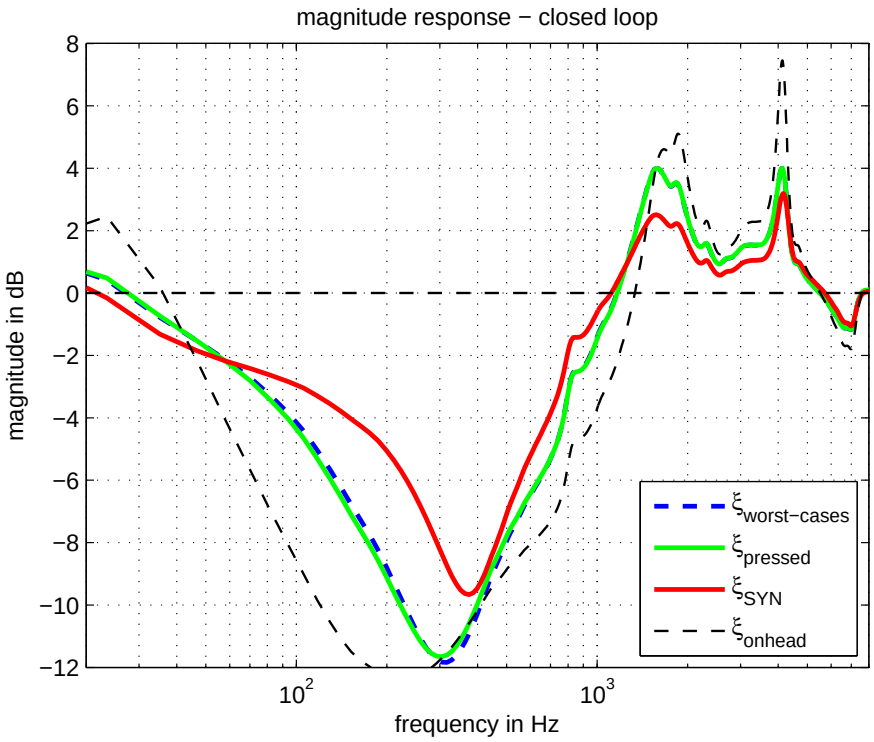

Figure 5.16: Performance analysis of 2nd order optimal filters applied to the pressed secondary path. The filter C_{onhead} which is only designed for the standard wearing situation violates the design constraint (i.e. $20 \log \max |\xi(s)| \leqslant 4\text{dB}$).

5.3.1 Summary

In feedback ANC headphones, the optimal control filter depends on the secondary path. The secondary path of a usual wearing situation is regarded as the nominal secondary path. However, the secondary path changes considerably if the headphones are lifted or pressed against the ears [Gul13]. It is therefore not sufficient to consider only the nominal secondary path in the constraints of the feedback filter optimization. To fulfill the constraints for all usage scenarios, the secondary paths which represent the worst-cases have to be considered.
Further, we can denote that it is necessary to include all worst-case constraints if we want to guarantee stability. From the magnitude and phase constraint for the control filter, it follows that the worst-case secondary paths are the ones which either show the largest magnitude or whose phase response is closest to -$\pi(2n-1)$ in some bandwidth.
It can be seen that the secondary path of the pressed headphones represents the worst-case in a broad bandwidth, but in general it has to be assumed that more than one secondary path measure has to be considered in the constraints of the filter optimization. This is especially true for the middle and high frequency band, where the phase of the shaped open loop crosses π several times.
In order to save computational time, one could synthesize a single frequency response that combines piecewise worst-case magnitude with worst-case phase responses (from all measured secondary paths). Consequently, this abstract frequency response gives more conservative constraints for the optimization task and yields a lower noise canceling performance. Since the optimization task hast to be done only once and off-line, it is preferably to spend more optimization time and to consider all worst-case secondary paths because the resulting performance can be increased by 2dB in almost the complete ANC bandwidth.

Chapter 6

Conclusion

The computer aided filter optimization for ANC feedback filters can be done by various approaches, some are mentioned and two are presented in detail within this thesis. The classic filter optimization approaches need plant modeling in the state-space domain or model matching to start with, which is an uneasy and unusual task for the filter design for ANC headphones. A more common method to describe the secondary path (i.e. the plant) is to do an impulse response measurement with an exponential sine sweep. The Fourier analysis of the impulse reponse gives us the frequency response of the system with information about the magnitude and phase behavior of a secondary path. The secondary path is defined by the transfer function from the loudspeaker to the microphone, which also includes the fitting of the headphones. This frequency response can then be used instead of a plant model - as used in classic control theory - to calculate an optimal filter for active noise control via the two presented optimization approaches in this thesis.

The first approach in the cepstral domain formulates the constraints as a linear combination. Because of this property the approach defines a linear optimization problem, which can be easily calculated with a mathematical solver on a modern computer. The optimization results in a global maximum for open-loop gain, which in turn leads to large ANC.

The second approach states the constraints in a nonlinear formulation in the complex plane. Due to the fact that an IIR filter with limited order is desired, the optimization problem is non-convex. Consequently, the optimization process might only converge to a local minimum, which is dependent on the initial value.

The guessing of the initial value can be quite tricky for a user who is not familiar with non-convex programming algorithms. This is quite a drawback for the second approach.

For the comparision of the two methods presented within this thesis, it can be stated that the first approach is quite intuitive from an engineers sight, because of the familiar design constraints known from manual ANC filter design. Another advantage of the first approach is that the optimization process results in a global minimum and therefore needs only one run-through to get to a desired optimal filter if the constraints are chosen correctly. The achieved frequency response of the optimal filter can be used as a design template for an analog filter or approximated with known methods like the proposed filter approximation algorithm by Steiglitz and McBride. Nevertheless, it is crucial to repeat the investigation of the closed-loop stability for the approximated filter.

It is shown within this work that including only one measurement of a nominal secondary path is insufficient for a typical ANC headphone. It is therefore proposed to include several worst-case misuse scenarios (i.e. fittings of the headphone, which are not intended by the manufacturer) into the optimization process to guarantee stability under all circumstances. The measurement results show that high magnitudes occur in most misuse scenarios over allmost the whole frequency range, especially for the cases when the headphone-cups are pressed against the users head. Also the phase response shows a faster falling phase than for a nominal secondary path (i.e. standard fitting case). Both facts limit the filter optimization in a manner that the system stability can be guaranteed in the case of misuse. It is nevertheless crucial to use measurements which represent reasonable misuse-scenarios that enhance the robust stability of the ANC feedback system.

Appendix A

Circle Intersections

Some of the relations of two intersecting circles can be formulated as

$$x = \frac{d^2 - r^2 + R^2}{2d} \tag{A.1}$$

$$a = \frac{1}{d}\sqrt{(-d + r - R)(-d - r + R)(-d + r + R)(d + r + R)} \tag{A.2}$$

$$\alpha = \arctan\frac{a/2}{x} \tag{A.3}$$

and are depicted in Fig. A.1.

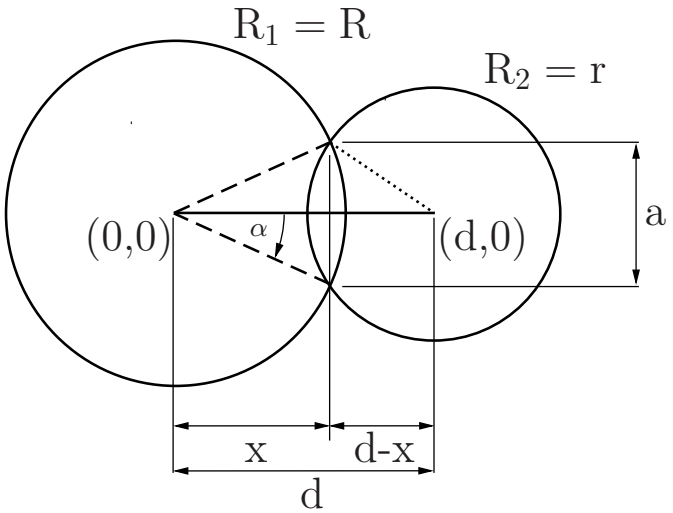

Figure A.1: Intersection of two circles and their mathematical relations to calculate the angle α.

Bibliography

[ÅM07] K. J. Åmström and R. M. Murray, "Feedback systems: An introduction for scientists and engineers," Tech. Rep., 2007.

[Cle72] H. Clemens, "Das Kopfgewicht des Menschen - ein biomechanisches problem," *Archiv für orthopädische und Unfall-Chirurgie, mit besonderer Berücksichtigung der Frakturenlehre und der orthopädisch-chirurgischen Technik*, vol. 73, no. 3, pp. 220–228, 1972.

[DFT91] J. C. Doyle, B. Francis, and A. Tannenbaum, *Feedback Control Theory*. Prentice Hall Professional Technical Reference, 1991.

[FK95] B. Francis and P. Khargonekar, *Robust control theory*, ser. The IMA volumes in mathematics and its applications. Springer-Verlag, 1995. [Online]. Available: http://books.google.at/books?id=81vvAAAAMAAJ

[FZ84] B. A. Francis and G. Zames, "On H_∞-optimal sensitivity theory for SISO feedback systems," *IEEE Transactions on Automatic Control*, vol. VOL. AC-29, 1984.

[GH13] M. Guldenschuh and R. Holdrich, "Prediction filter design for active noise cancellation headphones," *Signal Processing, IET*, vol. 7, no. 6, pp. 497–504, August 2013.

[GMK05] W. Gan, S. Mitra, and S. Kuo, "Adaptive feedback active noise control headset: implementation, evaluation and its extensions," *Consumer Electronics, IEEE Transactions on*, vol. 51, no. 3, pp. 975–982, Aug 2005.

[Gul13] M. Guldenschuh, "Secondary-path models in adaptive-noise-control headphones," in *Systems and Control (ICSC), 2013 3rd International Conference on*, Oct 2013, pp. 653–658.

[Gul14] ——, "Least-mean-square weighted parallel IIR filters in active noise control headphones," in *EUSIPCO, 2014 22nd European Signal Processing*, Sept. 2014.

[HD06] M. Horn and N. Dourdoumas, *Regelungstechnik: rechnerunterstützter Entwurf zeitkontinuierlicher und zeitdiskreter Regelkreise*, ser. Elektrotechnik : Regelungstechnik. Pearson Studium, 2006. [Online]. Available: http://books.google.at/books?id=1BgxPQAACAAJ

[HP09] B. Hua and I. Panahi, "Using a-weighting for psychoacoustic active noise control," in *Engineering in Medicine and Biology Society, 2009. EMBC 2009. Annual International Conference of the IEEE*, Sept 2009, pp. 5701–5704.

[Lar07] J. Laroche, "Optimal contraint-based loop-shaping in the cepstral domain," *IEEE Signal Processing Letters*, vol. 14, no. 4, 2007.

[Lue36] P. Lueg, "Process of silencing sound oscillations," June 1936, uS Patent 2,043,416. [Online]. Available: http://www.google.com/patents/US2043416

[OS89] A. V. Oppenheim and Schafer, *Discrete-time Signal Processing*. Englewood Cliffs, NJ, USA: Prentice-Hall, Inc., 1989.

[Paw02] M. Paweczyk, "Analogue active noise control," *Applied Acoustics*, vol. 63, no. 11, pp. 1193 – 1213, 2002. [Online]. Available: http://www.sciencedirect.com/science/article/pii/S0003682X02000270

[Pol84] E. Polak, "A modified nyquist stability test for use in computer-aided design," *Automatic Control, IEEE Transactions on*, vol. 29, no. 1, pp. 91–93, Jan 1984.

[RE99] B. Rafaely and S. J. Elliott, "H_2/H_∞ active control of sound in a headrest: Design and implementation," *IEEE Transactions on Control Systems Technology*, vol. 7, no. 1, 1999.

[SH01] S.Yu and J. Hu, "Controller design for active noise cancellation headphones using experimental raw data," *IEEE Transactions on Mechatronics*, vol. 6, no. 4, December 2001.

[SM65] K. Steiglitz and L. E. McBride, "A technique for the identification of linear systems," *IEEE Transactions on Automatic Control*, vol. AC-10, no. 4, pp. 461 – 464, 1965.

[Wik14] Wikipedia, "State space representation— Wikipedia, the free encyclopedia," September 2014. [Online]. Available: http://en.wikipedia.org/wiki/State_space_representation

[wm10] wolfson microelectronics, "Ambient noise-cancellation for headphones and handsets," August 2010. [Online]. Available: http://www.wolfsonmicro.com/media/77008/\Ambient_noise_cancellation_for_headphones_and_handsets.pdf

[Zam81] G. Zames, "Feedback and optimal sensitivity: Model reference transformations, multiplicative seminorms, and approximate inverses," *IEEE Transactions on Automatic Control*, vol. 26, no. 2, 1981.

[ZWQ12] L. Zhang, L. Wu, and X. Qiu, "An intuitive approach for feedback active noise controller design," *Applied Acoustics*, vol. 74, no. 1, pp. 160 – 168, 2012.